

# Channel Estimation for Hybrid MIMO Systems With Array Model Errors and Beam Squint Effects

Kabuto Arai, *Graduate Student Member, IEEE* and Koji Ishibashi, *Senior Member, IEEE*

**Abstract**—This paper proposes a channel estimation method for hybrid wideband multiple-input-multiple-output (MIMO) systems in high-frequency bands, including millimeter-wave (mmWave) and sub-terahertz (sub-THz), in the presence of beam squint effects and array errors arising from hardware impairments and environmental time fluctuations such as thermal effects and dynamic motion of the array. Although conventional channel estimation methods calibrate array errors through offline operation with large training pilots, the calibration errors remain due to time-varying array errors. Therefore, the proposed channel estimation method calibrates array errors online with small pilot overhead. In the proposed method, array response matrices are explicitly decomposed into a small number of physical parameters including path gains, angles and array errors, which are iteratively estimated by alternating optimization based on a maximum likelihood (ML) criterion. To enhance the convergence performance, we introduce a switching mechanism from an on-grid algorithm to an off-grid algorithm depending on the estimation accuracy of the array error during algorithmic iterations. Furthermore, we introduce an approximate mutual coupling model to reduce the number of parameters. The reduction of parameters not only lowers computational complexity but also mitigates overfitting to noisy observations. Numerical simulations demonstrate that the proposed method effectively works online even with small pilot overhead in the presence of array errors.

**Index Terms**—Channel estimation, millimeter-wave (mmWave), sub-terahertz (sub-THz), array errors, calibration, beam squint, compressed sensing.

## I. INTRODUCTION

As the demand for broadband communication grows, high carrier frequencies, such as millimeter-wave (mmWave) and sub-terahertz (sub-THz), are becoming increasingly important for future communication systems [2], [3]. However, these high-frequency bands experience significant attenuation due to weak diffraction, blockages and molecular absorption [4], [5]. To mitigate these challenges, beamforming techniques are extensively employed with massive antenna arrays, leveraging the short wavelengths of these high-frequency bands. In terms of cost and power consumption, hybrid beamforming architectures, which utilize both analog and digital precoders/combiners, are widely adopted instead of full-digital architectures [6], [7]. To design the optimal precoder and combiner for maximizing beamforming gain, channel state

information (CSI) is essential [8]–[10]. However, channel estimation in a hybrid beamforming architecture requires a large number of pilots during the training beam search process because the number of radio-frequency (RF) chains is much smaller than the number of antennas [11], [12].

To address the pilot overhead issue in wideband hybrid multiple-input-multiple-output (MIMO) systems, channel estimation methods based on compressed sensing (CS) techniques have been proposed [12]–[14]. These methods can significantly reduce pilot overhead by exploiting channel sparsity in the angle domain. To effectively leverage this sparsity, the virtual channel representation is widely utilized with a dictionary matrix, which is an array response matrix over a set of quantized angle grid points covering the entire angle domain. Since the dictionary matrix is based on the ideal array manifold model without accounting for modeling errors, the estimation performance of CS-based methods is adversely affected by modeling errors caused by array errors [15] in practical wideband hybrid MIMO systems [16]–[19].

The array errors arise from the following three factors [15]–[19]: (1) mutual coupling between antenna elements due to closely implemented massive antenna elements, causing unwanted energy interactions between the elements, (2) gain and phase errors in antenna elements resulting from the nonuniform electrical characteristics of individual devices and (3) antenna positioning errors stemming from the limited accuracy of manufacturing, especially in high-frequency bands because the wavelength is on the millimeter or micrometer scale in mmWave and sub-THz. These array errors introduce modeling errors, which severely degrade channel estimation performance because the CS-based channel estimation methods heavily rely on the ideal array model. Therefore, it is necessary to calibrate the array errors for accurate channel estimation.

The array errors are attributed not only to static factors, such as manufacturing errors, but also to time-varying factors, such as dynamic motion of the antenna arrays, aging of components and heat dissipation of electronic devices [20], [21]. Due to heat dissipation in the device, the electrical characteristics of devices change, resulting in non-uniform gain and phase characteristics in each antenna element. Moreover, these effects cause a deformation of the array structure with offset from the ideal antenna positions, leading to changes in mutual coupling. Even a slight change in antenna position on the order of a fraction of the wavelength can significantly deteriorate the performance of array signal processing, such as channel estimation [16]–[19] and beamforming [22]. Thus, the impact of array deformation becomes more pronounced at higher frequencies (i.e., with shorter wavelengths). Furthermore, in

This work was supported in part by Japan Science and Technology Agency (JST) Advanced International Collaborative Research Program (AdCORP) under Grant JPMJKB2307. An earlier version of this paper was presented in part at the 2023 IEEE 98th Vehicular Technology Conference (VTC2023-Fall) [DOI: 10.1109/VTC2023-Fall60731.2023.10333598.]. K. Arai and K. Ishibashi are with the Advanced Wireless and Communication Research Center (AWCC), The University of Electro-Communications, Tokyo 182-8285, Japan (e-mail: k.arai@awcc.uec.ac.jp, koji@ieec.org)

various communication scenarios, such as high-speed aircraft flight with dynamic wind loads [22], [23], satellite phased array [24] and wearable array antennas [25], [26], the array structure is deformed with time due to the motion of the array and fluctuations in surrounding environmental loads including temperature and pressure. Another scenario involving array deformation is movable antenna (MA) systems [27], [28], including fluid antenna (FA) systems [29], [30], where the antenna position is flexibly controlled to exploit spatial channel variation, known as spatial degrees of freedom (DoF). However, due to limited position control accuracy, antenna spacing errors remain. Moreover, mutual coupling changes with each adjustment of the antenna position, requiring frequent calibration after every adjustment. For the above reasons, frequent and fast calibration to mitigate time-varying array errors is needed [22], [31].

To compensate for array errors, various classic calibration methods have been proposed in the field of array signal processing [32]–[35]. In these methods, array errors, such as mutual coupling, phase/gain errors, and antenna spacing errors, are jointly estimated using calibration sources that is located at known positions and transmit reference signals for calibration through offline operation. Despite achieving high estimation performance, these approaches are time-consuming and costly due to the requirement of calibration sources. Additionally, the offline calibration is unable to address the time-varying array errors. To address these limitations, blind calibration techniques without calibration sources have been proposed [35]–[37]. These methods can jointly estimate both array errors and angles of arrivals (AoAs) from unknown sources. However, these methods assume narrow-band fully-digital array architectures, focusing only on the receiver side for AoA estimation. As a result, it is challenging to directly extend these methods to channel estimation algorithms in the considered communication systems operating at high carrier frequencies with wide bandwidth and hybrid array architectures that include both the transmitter and receiver.

To calibrate array errors in wideband hybrid MIMO systems without calibration sources, channel estimation methods based on dictionary learning techniques have been proposed [16], [17], [19]. The authors of [16] proposed the combined dictionary learning (CoDL) algorithm, where a combined dictionary matrix, including array errors at both the transmitter and receiver sides, is updated to calibrate these array errors with training pilots. While these dictionary learning methods do not require for calibration sources, they require a large number of pilots to achieve sufficient channel estimation performance, since the dictionary matrix contains numerous unknown parameters to be estimated. Therefore, these works [16], [17], [19] assume that the dictionary learning is performed offline with a large number of training pilots, after which channel estimation is performed online with a small number of pilots using the updated dictionary matrix. However, the channel estimation performance using the dictionary matrix trained offline degrades since array errors change with time [20]–[31]. If the dictionary is updated online, a significant number of pilots is required at each channel coherence time, which defeats the original purpose of CS-based channel estimation

in reducing pilot overhead.

In addition, due to the significant increase in bandwidth and antenna aperture, the beam squint effect [38], also known as the spatial wideband effect [39], becomes non-negligible in high-frequency bands, where the array responses for AoAs and angles of departures (AoDs) depend on frequency. Although many studies [40]–[42] have proposed channel estimation methods based on CS algorithms to reduce pilot overhead, these methods typically address only beam squint effects and neglect array errors. To overcome this limitation, the authors in [18] proposed the dictionary learning for hardware impairments under beam squint (DLHWBS) algorithm, which considers both array errors and beam squint effects by accounting for the frequency-dependent array response. However, this dictionary learning method also relies on offline calibration, requiring a large number of training pilots, similar to conventional methods [16], [17], [19]. Consequently, the pilot overhead problem remains unresolved in scenarios involving both time-varying array errors and beam squint effects.

In light of the above issues, we propose a channel estimation method considering time-varying array errors and beam squint effects by online calibration with small pilot overhead. The proposed method can be applied to wideband MIMO systems with hybrid architectures, where array errors and beam squint effects occur on both the transmitter and receiver sides. Our major contributions are summarized as follows:

- The proposed channel estimation is operated online with small pilot overhead for array error calibration by decomposing the dictionary matrix containing many unknown parameters into a smaller number of physical parameters constituting the channel matrix, which include AoAs, AoDs, path gains and array errors, based on the array structure. Unlike the conventional dictionary learning methods [16]–[19], which directly update the dictionary matrix with high-dimensional parameters, the proposed method estimates a smaller number of parameters owing to this decomposition. The decomposed parameters are estimated using an alternating optimization technique [43] based on a maximum likelihood (ML) criteria, where each parameter is estimated iteratively with the other parameters fixed as tentative estimates.
- To enhance convergence performance in the alternating optimization, we introduce a switching mechanism from an on-grid algorithm, based on a CS method, to an off-grid algorithm, based on a gradient decent method, for estimating AoAs, AoDs, and path gains. During early iterations when the estimation accuracy for array errors is limited, an on-grid algorithm is applied to avoid convergence to a local optimum. In subsequent later iterations with the higher estimation accuracy for array errors, an off-grid algorithm is employed to finely estimate AoAs and AoDs without angle grids. Considering beam squint effects, the distributed compressed sensing-simultaneous orthogonal matching pursuit (DCS-SOMP) algorithm [44] is applied as an on-grid method, leveraging the common support property arising from AoAs and AoDs shared across all subcarriers in the frequency-dependent dictionary matrix.

- To enhance channel estimation performance and reduce computational complexity, an approximate mutual coupling model is introduced. Although the mutual coupling matrix can be modeled as a symmetric Toeplitz matrix in the case of uniform linear array (ULA) [36], the antenna spacing errors distort the Toeplitz structure in practical systems. To account for this distortion, the proposed method approximately decomposes the mutual coupling matrix into a non-Toeplitz part and a Toeplitz part. Among the elements in the mutual coupling matrix, only a few elements that have significant impact on estimation performance are exactly modeled with a non-Toeplitz structure, while the remaining elements are approximately modeled with a Toeplitz structure. This approximate decomposition reduces the number of unknown parameters in the mutual coupling matrix compared to an exact model without a Toeplitz structure. Consequently, reducing the number of parameters not only lowers computational complexity but also helps avoid overfitting to noisy observations when the number of training pilots is limited in a low SNR region.

The rest of the paper is organized as follows: Section II describes channel model including array errors and beam squint effects, and formulates signal model for channel estimation in a wideband hybrid MIMO system. Section III illustrates the proposed channel estimation algorithm based on an alternating optimization technique. Section IV provide numerical results. Finally, the conclusions are reported in Section V.

*Notation:* Throughout this paper, the following notations are used. A vector and matrix are represented by boldfaced lowercase letter  $\mathbf{a}$  and uppercase letter  $\mathbf{A}$ . The operators  $(\cdot)^*$ ,  $(\cdot)^T$  and  $(\cdot)^H$  indicate conjugate, transpose and conjugate transpose, respectively.  $\mathbf{I}_N$  and  $\mathbf{0}_{N \times M}$  indicate the  $N \times N$  identity matrix and  $N \times M$  zero matrix, respectively. A diagonal matrix consisting of elements of a vector  $\mathbf{x} = [x_1, \dots, x_N]^T$  is represented as  $\text{diag}(\mathbf{x})$ . The notation  $[\mathbf{A}]_{i,j}$  and  $[\mathbf{A}]_{:,j}$  indicate the  $(i, j)$  element and the  $j$ -th column vector of the matrix  $\mathbf{A}$ , respectively. The operators  $\odot$ ,  $\otimes$  and  $\circ$  represent Hadamard, Kronecker and Khatri-Rao product for any vectors or matrices, respectively. For any vector  $\mathbf{a}$  and matrix  $\mathbf{A}$ ,  $\|\mathbf{a}\|_p$  and  $\|\mathbf{A}\|_F$  indicate  $p$ -norm and Frobenius norm, respectively.  $\Re[\mathbf{A}]$ ,  $\mathbf{A}^\dagger$  and  $\text{vec}(\mathbf{A})$  denote the real part, pseudo-inverse matrix and vectorization of the matrix  $\mathbf{A}$ .  $\mathcal{CN}(\boldsymbol{\mu}, \mathbf{C})$  denote a circularly symmetric complex Gaussian distribution with mean  $\boldsymbol{\mu}$  and covariance  $\mathbf{C}$ . For a vector  $\boldsymbol{\theta} = [\theta_1, \dots, \theta_N]^T$ ,  $\sin \boldsymbol{\theta}$  denotes the corresponding vector  $[\sin \theta_1, \dots, \sin \theta_N]^T$ .

## II. SYSTEM MODEL

We consider an uplink MIMO orthogonal frequency division multiplexing (OFDM) system, where a base station (BS) and a user equipment (UE) employ hybrid MIMO architectures with a ULA equipped with  $N_r$  and  $N_t$  antennas and  $N_{r,\text{RF}}$  and  $N_{t,\text{RF}}$  RF chains, respectively. The carrier frequency, the system bandwidth, and the number of subcarriers are denoted by  $f_c$ ,  $B$  and  $K$ , respectively. The carrier wavelength are denoted by  $\lambda_c = f_c/c$  with the speed of light  $c$ . The  $k$ -th subcarrier  $f_k$  is given by  $f_k = f_c + \Delta f_k$  with  $\Delta f_k = -B/2 + (k-1)B/K$ ,  $k \in \{1, 2, \dots, K\}$ .

### A. Channel Model in MIMO-OFDM System

We consider a channel model with the frequency-wideband effect and the spatial wideband effect also known as the dual-wideband effect [40]–[42]. The channel is composed of  $L$  resolvable paths. For the  $l$ -th path,  $\alpha_l$ ,  $\tau_l$ ,  $\phi_l$ ,  $\theta_l$  are the complex path gain, time delay, AoA and AoD, respectively. Then, the channel matrix between the BS and UE at the  $k$ -th subcarrier is expressed as <sup>1</sup>

$$\mathbf{H}_k = \sum_{l=1}^L \alpha_l e^{-j2\pi\Delta f_k \tau_l} \check{\mathbf{a}}_{r,k}(\phi_l) \check{\mathbf{a}}_{t,k}(\theta_l)^H, \quad (1)$$

where  $\check{\mathbf{a}}_{r,k}(\phi_l) \in \mathbb{C}^{N_r \times 1}$  and  $\check{\mathbf{a}}_{t,k}(\theta_l) \in \mathbb{C}^{N_t \times 1}$  are the array response vector including array errors such as mutual coupling, gain/phase errors and antenna spacing errors at the BS and UE sides. These array response vectors are given by

$$\check{\mathbf{a}}_{r,k}(\phi_l) = \mathbf{C}_r \boldsymbol{\Gamma}_r \mathbf{a}_{r,k}(\phi_l, \boldsymbol{\varepsilon}_r), \quad (2)$$

$$\check{\mathbf{a}}_{t,k}(\theta_l) = \mathbf{C}_t \boldsymbol{\Gamma}_t \mathbf{a}_{t,k}(\theta_l, \boldsymbol{\varepsilon}_t), \quad (3)$$

where  $\mathbf{a}_{r,k}(\phi_l, \boldsymbol{\varepsilon}_r) \in \mathbb{C}^{N_r \times 1}$  and  $\mathbf{a}_{t,k}(\theta_l, \boldsymbol{\varepsilon}_t) \in \mathbb{C}^{N_t \times 1}$  are the array response vectors including antenna spacing errors  $\boldsymbol{\varepsilon}_r$  and  $\boldsymbol{\varepsilon}_t$ . The  $n_r$ -th element of  $\mathbf{a}_{r,k}(\phi_l, \boldsymbol{\varepsilon}_r)$  and the  $n_t$ -th element of  $\mathbf{a}_{t,k}(\theta_l, \boldsymbol{\varepsilon}_t)$  are expressed as

$$[\mathbf{a}_{r,k}(\phi_l, \boldsymbol{\varepsilon}_r)]_{n_r} = e^{j\frac{2\pi}{\lambda_c} \left(1 + \frac{\Delta f_k}{f_c}\right) \{(n_r-1)d_r + \varepsilon_{n_r}\} \sin(\phi_l)}, \quad (4)$$

$$[\mathbf{a}_{t,k}(\theta_l, \boldsymbol{\varepsilon}_t)]_{n_t} = e^{j\frac{2\pi}{\lambda_c} \left(1 + \frac{\Delta f_k}{f_c}\right) \{(n_t-1)d_t + \varepsilon_{n_t}\} \sin(\theta_l)}, \quad (5)$$

where  $d_r$ ,  $d_t$  are the ideal antenna spacing at the BS and UE sides, respectively. Due to the beam squint effect also known as spatial wideband effect [40]–[42], the array response vectors in (4) and (5) depend on the subcarrier index  $k$  because the approximation  $\Delta f_k/f_c \simeq 0$  does not hold unlike the conventional MIMO systems [12], [16].

In (2) and (3),  $\boldsymbol{\Gamma}_r \triangleq \text{diag}(\boldsymbol{\gamma}_r) \in \mathbb{C}^{N_r \times N_r}$ , and  $\boldsymbol{\Gamma}_t \triangleq \text{diag}(\boldsymbol{\gamma}_t) \in \mathbb{C}^{N_t \times N_t}$  are the antenna gain/phase error matrices with  $\boldsymbol{\gamma}_r \triangleq [g_{r,1} e^{j\nu_{r,1}}, \dots, g_{r,N_r} e^{j\nu_{r,N_r}}]^T \in \mathbb{C}^{N_r \times 1}$ , and  $\boldsymbol{\gamma}_t \triangleq [g_{t,1} e^{j\nu_{t,1}}, \dots, g_{t,N_t} e^{j\nu_{t,N_t}}]^T \in \mathbb{C}^{N_t \times 1}$ , where  $\{g_{r,n_r}, \nu_{r,n_r}\}$  and  $\{g_{t,n_t}, \nu_{t,n_t}\}$  denote the gain and phase errors at the  $n_r$ -th BS antenna and the  $n_t$ -th UE antenna, respectively.  $\mathbf{C}_r \in \mathbb{C}^{N_r \times N_r}$  and  $\mathbf{C}_t \in \mathbb{C}^{N_t \times N_t}$  are the mutual coupling matrices. The mutual coupling matrix is ideally modeled by a symmetric Toeplitz matrix in the ULA configuration [36]. However, the antenna spacing errors  $\boldsymbol{\varepsilon}_r$  and  $\boldsymbol{\varepsilon}_t$  distort the mutual coupling effects. Therefore, calibration methods under the assumption of the symmetric Toeplitz structure leads to the performance deterioration due to the modeling errors. Thus, this paper considers the modeling errors as will be described in Section III-B.

By denoting the equivalent path gain at the  $k$ -th subcarrier as  $\mathbf{z}_k \triangleq [z_{1,k}, \dots, z_{L,k}]^T \in \mathbb{C}^{L \times 1}$  with  $z_{k,l} \triangleq \alpha_l e^{-j2\pi\Delta f_k \tau_l}$ , the channel matrix at the  $k$ -th subcarrier in (1) is expressed as

$$\mathbf{H}_k = \check{\mathbf{A}}_{r,k}(\boldsymbol{\phi}) \text{diag}(\mathbf{z}_k) \check{\mathbf{A}}_{r,k}^H(\boldsymbol{\theta}), \quad (6)$$

<sup>1</sup>Although the author in [18] considers the effect of pulse shaping for band-limitation, we assume ideal band-limitation in the OFDM system, as its impact is negligible for channel estimation performance, as in [40]–[42].

where  $\check{\mathbf{A}}_{r,k}(\phi) \triangleq [\check{\mathbf{a}}_{r,k}(\phi_1) \cdots \check{\mathbf{a}}_{r,k}(\phi_L)] \in \mathbb{C}^{N_r \times L}$  and  $\check{\mathbf{A}}_{t,k}(\theta) \triangleq [\check{\mathbf{a}}_{t,k}(\theta_1) \cdots \check{\mathbf{a}}_{t,k}(\theta_L)] \in \mathbb{C}^{N_t \times L}$  are the array response matrices including all array errors with AoAs  $\phi \triangleq \{\phi_l\}_{l=1}^L$  and AoDs  $\theta \triangleq \{\theta_l\}_{l=1}^L$ . For the sake of notation convenience, the array response matrices including antenna spacing errors at the BS and UE are defined as  $\mathbf{A}_{r,k}(\phi, \varepsilon_r) \triangleq [\mathbf{a}_{r,k}(\phi_1, \varepsilon_r) \cdots \mathbf{a}_{r,k}(\phi_L, \varepsilon_r)] \in \mathbb{C}^{N_r \times L}$  and  $\mathbf{A}_{t,k}(\theta, \varepsilon_t) \triangleq [\mathbf{a}_{t,k}(\theta_1, \varepsilon_t) \cdots \mathbf{a}_{t,k}(\theta_L, \varepsilon_t)] \in \mathbb{C}^{N_t \times L}$ , which satisfy  $\check{\mathbf{A}}_{r,k}(\phi) = \mathbf{C}_r \mathbf{\Gamma}_r \mathbf{A}_{r,k}(\phi, \varepsilon_r)$  and  $\check{\mathbf{A}}_{t,k}(\theta) = \mathbf{C}_t \mathbf{\Gamma}_t \mathbf{A}_{t,k}(\theta, \varepsilon_t)$ .

Based on the property of vectorization,  $\text{vec}(\mathbf{A} \text{diag}(\mathbf{b}) \mathbf{C}) = (\mathbf{C}^T \circ \mathbf{A}) \mathbf{b}$  for any matrices  $\mathbf{A}$  and  $\mathbf{C}$  and a vector  $\mathbf{b}$ , the vectorized channel at the  $k$ -th subcarrier  $\mathbf{h}_k \triangleq \text{vec}(\mathbf{H}_k) \in \mathbb{C}^{N_r N_t \times 1}$  is given by

$$\mathbf{h}_k = \underbrace{\{\check{\mathbf{A}}_{r,k}(\phi) \circ \check{\mathbf{A}}_{t,k}(\theta)\}}_{\triangleq \Psi \in \mathbb{C}^{N_r N_t \times L}} \mathbf{z}_k. \quad (7)$$

### B. Received Signal Model in Hybrid MIMO-OFDM System

To estimate the channel matrix, the UE transmits pilot signal with the pilot length  $N_p$  to the BS in every training frame. We assume that AoAs, AoDs, and path gains randomly change in every frame, while the array errors remain constant over the total  $M$  frames. Therefore, the BS calibrates the array errors using the pilot signals from the total  $M$  training frames as in [16]–[18]. For the  $m$ -th training frame, let  $\mathbf{H}_k^{(m)}$ ,  $\theta^{(m)}$ ,  $\phi^{(m)}$ , and  $\mathbf{z}_k^{(m)}$  denote the channel matrix, AoAs, AoDs, and path gains, respectively.

Let  $p \in \{1, 2, \dots, N_p\}$  denotes the pilot index. For the  $p$ -th pilot,  $\mathbf{q}_p \in \mathbb{C}^{N_t, \text{RF}}$  denotes the pilot signal generated by quadrature phase-shift keying (QPSK), satisfying  $\mathbb{E}[\mathbf{q}_p \mathbf{q}_p^H] = P_s \mathbf{I}_{N_t, \text{RF}}$  with the transmitted power  $P_s$ .  $\bar{\mathbf{W}}_p \in \mathbb{C}^{N_r \times N_t, \text{RF}}$  and  $\mathbf{F}_p \in \mathbb{C}^{N_t \times N_t, \text{RF}}$  are the analog training combiner and precoder, designed as [12], [42],

$$[\mathbf{W}_p]_{i,j} = \frac{1}{\sqrt{N_r}} \exp(j\varphi_{r,i,j}), \quad (8)$$

$$[\mathbf{F}_p]_{i,j} = \frac{1}{\sqrt{N_t}} \exp(j\varphi_{t,i,j}), \quad (9)$$

where  $\varphi_{r,i,j}$  and  $\varphi_{t,i,j}$  are uniformly randomly chosen from the quantized phase set  $\{0, 2\pi/2^{N_Q}, 6\pi/2^{N_Q}, \dots, 2\pi(2^{N_Q} - 1)/2^{N_Q}\}$  with  $N_Q$  quantization bits. Then, the received pilot signal at the  $p$ -th pilot, the  $k$ -th subcarrier, and the  $m$ -th training frame,  $\bar{\mathbf{y}}_{p,k}^{(m)} \in \mathbb{C}^{N_r, \text{RF}} \times 1$  is expressed as

$$\bar{\mathbf{y}}_{p,k}^{(m)} = \bar{\mathbf{W}}_p \mathbf{H}_k^{(m)} \mathbf{F}_p \mathbf{q}_p + \bar{\mathbf{W}}_p \bar{\mathbf{n}}_{p,k}^{(m)}, \quad (10)$$

where  $\bar{\mathbf{n}}_{p,k}^{(m)} \in \mathbb{C}^{N_r, \text{RF}} \times 1$  is an additive noise vector that follows  $\mathcal{CN}(\mathbf{0}_{N_r, \text{RF}} \times 1, \sigma^2 \mathbf{I}_{N_r, \text{RF}})$  with noise variance  $\sigma^2$ .

Since the combined noise vector  $\bar{\mathbf{W}}_p \bar{\mathbf{n}}_{p,k}^{(m)}$  in (10) follows  $\mathcal{CN}(\mathbf{0}_{N_r, \text{RF}} \times 1, \mathbf{C}_p)$  with the covariance matrix  $\mathbf{C}_p = \sigma^2 \bar{\mathbf{W}}_p \bar{\mathbf{W}}_p^H$ , the received signal should be whitened by the pre-whitening matrix  $\mathbf{D}_p = \sigma \mathbf{C}_p^{-\frac{1}{2}}$ . Then, the whitened received signal  $\mathbf{y}_{p,k}^{(m)} \triangleq \mathbf{D}_p \bar{\mathbf{y}}_{p,k}^{(m)} \in \mathbb{C}^{N_r, \text{RF}} \times 1$  is given by

$$\mathbf{y}_{p,k}^{(m)} = \mathbf{W}_p \mathbf{H}_k^{(m)} \mathbf{F}_p \mathbf{q}_p + \mathbf{n}_{p,k}^{(m)}, \quad (11)$$

where  $\mathbf{n}_{p,k}^{(m)} = \mathbf{D}_p \bar{\mathbf{W}}_p \bar{\mathbf{n}}_{p,k}^{(m)}$  is the whitened noise vector that follows  $\mathcal{CN}(0, \sigma^2 \mathbf{I}_{N_r, \text{RF}})$  and  $\mathbf{W}_p \triangleq \mathbf{D}_p \bar{\mathbf{W}}_p$  is the whitened analog combiner.

Using the property of vectorization and Kronecker-product,  $\text{vec}(\mathbf{A} \mathbf{X} \mathbf{C}) = (\mathbf{C}^T \otimes \mathbf{A}) \text{vec}(\mathbf{X})$  for any matrices  $\mathbf{A}$ ,  $\mathbf{X}$ , and  $\mathbf{C}$ , the received signal  $\mathbf{y}_{p,k}^{(m)}$  in (11) can be reformulated as

$$\mathbf{y}_{p,k}^{(m)} = \underbrace{(\mathbf{q}_p^T \mathbf{F}_p^T \otimes \mathbf{W}_p)}_{\triangleq \Phi_p \in \mathbb{C}^{N_r, \text{RF}} \times N_r N_t} \mathbf{h}_k^{(m)} + \mathbf{n}_{p,k}^{(m)}, \quad (12)$$

where  $\mathbf{h}_k^{(m)} = \text{vec}(\mathbf{H}_k^{(m)})$  is the vectorized channel defined in (7), and  $\Phi_p \triangleq \mathbf{q}_p^T \mathbf{F}_p^T \otimes \mathbf{W}_p \in \mathbb{C}^{N_r, \text{RF}} \times N_t N_r$  is the training beam matrix at the  $p$ -th pilot.

Stacking  $\mathbf{y}_{p,k}^{(m)}$  over  $N_p$  pilots in the row direction, the received signal in (12) can be extended as

$$\underbrace{\begin{bmatrix} \mathbf{y}_{1,k}^{(m)} \\ \vdots \\ \mathbf{y}_{N_p,k}^{(m)} \end{bmatrix}}_{\triangleq \mathbf{y}_k^{(m)}} = \underbrace{\begin{bmatrix} \Phi_1 \\ \vdots \\ \Phi_{N_p} \end{bmatrix}}_{\triangleq \Phi} \mathbf{h}_k^{(m)} + \underbrace{\begin{bmatrix} \mathbf{n}_{1,k}^{(m)} \\ \vdots \\ \mathbf{n}_{N_p,k}^{(m)} \end{bmatrix}}_{\triangleq \mathbf{n}_k^{(m)}}, \quad (13)$$

where  $\mathbf{y}_k^{(m)} \in \mathbb{C}^{N_r, \text{RF}} N_p \times 1$ ,  $\mathbf{n}_k^{(m)} \in \mathbb{C}^{N_r, \text{RF}} N_p \times 1$  and  $\Phi \in \mathbb{C}^{N_r, \text{RF}} N_p \times N_t N_r$  are the received signal, noise vector and training beam matrix, including  $N_p$  pilots.

### C. Channel Estimation Without Considering Array Errors

In order to accurately estimate the channel vector  $\mathbf{h}_k^{(m)}$  based on the measurement equation (13) using classical channel estimation methods, such as least square (LS), the number of pilots must satisfy  $N_p \geq \frac{N_t N_r}{N_r, \text{RF}}$ . This requirement results in an increase in pilot overhead as the number of antennas grows, especially in hybrid MIMO systems at high carrier frequencies.

To reduce pilot overhead, channel estimation methods to exploit the channel sparsity in the angular domain have been proposed in [6], [12], [40]–[42], based on a CS framework. These methods utilize virtual array representation with the AoA and AoD grids, generated by spatially quantizing the angle domain into  $G_\phi$  and  $G_\theta$  points as  $\tilde{\phi} \triangleq \{\tilde{\phi}_{g_\phi}\}_{g_\phi=1}^{G_\phi}$  and  $\tilde{\theta} \triangleq \{\tilde{\theta}_{g_\theta}\}_{g_\theta=1}^{G_\theta}$ , with each grid  $\tilde{\phi}_{g_\phi}, \tilde{\theta}_{g_\theta} \in [-\pi/2, \pi/2]$ . Using the virtual array responses  $\check{\mathbf{A}}_{r,k}(\tilde{\phi}) \in \mathbb{C}^{N_r \times G_\phi}$  and  $\check{\mathbf{A}}_{t,k}(\tilde{\theta}) \in \mathbb{C}^{N_t \times G_\theta}$  based on the angle grids, the channel vector in (7) can be approximated as

$$\mathbf{h}_k^{(m)} \simeq \left\{ \check{\mathbf{A}}_{r,k}(\tilde{\phi}) \otimes \check{\mathbf{A}}_{t,k}(\tilde{\theta}) \right\} \tilde{\mathbf{z}}_k^{(m)} = \tilde{\Psi}_k \tilde{\mathbf{z}}_k^{(m)}, \quad (14)$$

where  $\tilde{\Psi}_k \triangleq \check{\mathbf{A}}_{r,k}(\tilde{\phi}) \otimes \check{\mathbf{A}}_{t,k}(\tilde{\theta}) \in \mathbb{C}^{N_r N_t \times G_\phi G_\theta}$  is the dictionary matrix, and  $\tilde{\mathbf{z}}_k^{(m)} \in \mathbb{C}^{G_\phi G_\theta \times 1}$  is the sparse path gain vector corresponding to AoA and AoD grids.

Substituting (14) into (13), the measurement equation can be reformulated as

$$\mathbf{y}_k^{(m)} \simeq \Phi \tilde{\Psi}_k \tilde{\mathbf{z}}_k^{(m)} + \mathbf{n}_k^{(m)}. \quad (15)$$

Based on the measurement equation (15), the channel vector  $\mathbf{h}_k^{(m)}$  can be estimated with small pilot overhead by a CS algorithm to rely on the sparsity of  $\tilde{\mathbf{z}}_k^{(m)}$ . However, since the array responses  $\check{\mathbf{A}}_{r,k}$  and  $\check{\mathbf{A}}_{t,k}$  include array errors

$\{\mathbf{C}_r, \mathbf{C}_t, \mathbf{\Gamma}_r, \mathbf{\Gamma}_t, \boldsymbol{\varepsilon}_r, \boldsymbol{\varepsilon}_t\}$ , the dictionary matrix  $\tilde{\Psi}_k$  cannot be designed. Therefore, many works design the dictionary matrix  $\tilde{\Psi}_k$  under the assumption that array errors do not exist (i.e.,  $\mathbf{C}_r = \mathbf{\Gamma}_r = \mathbf{I}_{N_r}$ ,  $\mathbf{C}_t = \mathbf{\Gamma}_t = \mathbf{I}_{N_t}$ ,  $\boldsymbol{\varepsilon}_r = \mathbf{0}_{N_r \times 1}$ ,  $\boldsymbol{\varepsilon}_t = \mathbf{0}_{N_t \times 1}$ ). This assumption causes severe performance deterioration due to model mismatch when using a CS algorithm. Therefore, it is necessary to compensate for array errors while estimating AoAs, AoDs and path gains to improve channel estimation performance.

### III. PROPOSED CHANNEL ESTIMATION ALGORITHM

This section describes the proposed channel estimation algorithm considering array errors and beam squint effects. As described in Section II-C, channel estimation performance based on a CS framework is limited due to array errors. To address this issue, the authors in [16]–[18] proposed dictionary learning methods where the path gain matrix  $\tilde{\mathbf{Z}}^{(m)} \triangleq [\tilde{\mathbf{z}}_1^{(m)}, \dots, \tilde{\mathbf{z}}_K^{(m)}]$  and the dictionary matrix  $\tilde{\Psi}_k$ , which includes array errors, are alternately updated in an iterative manner. These approaches, however, cause substantial pilot overhead to accurately update the dictionary matrix, primarily due to the large dimension of the dictionary. Therefore, the proposed method explicitly decomposes the dictionary matrix into a smaller number of physical parameters constituting the channel, based on the array structure, and estimates these parameters instead of directly estimating the dictionary. Owing to the smaller size of the parameters compared to the dictionary, the required pilot overhead is consequently reduced.

From (7) and (14), the channel vector is composed of the unknown parameters  $\boldsymbol{\Omega} \triangleq \{\mathbf{C}_r, \mathbf{C}_t, \mathbf{\Gamma}_r, \mathbf{\Gamma}_t, \boldsymbol{\varepsilon}_r, \boldsymbol{\varepsilon}_t, \{\boldsymbol{\phi}^{(m)}, \boldsymbol{\theta}^{(m)}, \mathbf{Z}^{(m)}\}_{m=1}^M\}$ . In the proposed methods, these unknown parameters are alternately estimated based on a ML criterion without directly estimating the dictionary matrix.

From (7) and (12), the conditional probability density function (PDF) given the unknown parameter set  $\boldsymbol{\Omega}$  is written by

$$p(\mathbf{y}_{p,k}^{(m)} | \boldsymbol{\Omega}) = \mathcal{CN}(\Phi_p \Psi \mathbf{z}_k, \sigma^2 \mathbf{I}_{N_r, \text{RF}}). \quad (16)$$

Since the log likelihood function  $\mathcal{L}(\boldsymbol{\Omega})$  can be expressed as

$$\mathcal{L}(\boldsymbol{\Omega}) = \sum_{m=1}^M \sum_{p=1}^{N_p} \sum_{k=1}^K \ln p(\mathbf{y}_{p,k}^{(m)} | \boldsymbol{\Omega}), \quad (17)$$

the ML problem can be formulated as the minimization problem (18) in the top of next page.

Since the objective function  $\mathcal{F}(\boldsymbol{\Omega})$  is not jointly convex for the unknown parameter set  $\boldsymbol{\Omega}$ , we employ an alternating optimization technique, where each parameter is iteratively updated with the other parameters fixed as tentative estimates. As described in the following subsections, the estimates for  $\hat{\mathbf{z}}_k^{(m)}$ ,  $\hat{\mathbf{C}}_r$ ,  $\hat{\mathbf{C}}_t$ ,  $\hat{\mathbf{\Gamma}}_r$ , and  $\hat{\mathbf{\Gamma}}_t$  are obtained in closed-form expressions owing to the convexity of the objective function for each parameter in the alternating minimization process. In contrast, since the objective function is not convex with respect to  $\boldsymbol{\phi}^{(m)}$ ,  $\boldsymbol{\theta}^{(m)}$ ,  $\boldsymbol{\varepsilon}_r$ , and  $\boldsymbol{\varepsilon}_t$ , these parameters are updated via a gradient descent approach or a CS-based method.

The following subsections describe the estimation method for each parameter, given the other tentative estimates. As for

the initial tentative estimates in the algorithmic iteration, these parameters are set to  $\hat{\mathbf{C}}_r = \hat{\mathbf{\Gamma}}_r = \mathbf{I}_{N_r}$ ,  $\hat{\mathbf{C}}_t = \hat{\mathbf{\Gamma}}_t = \mathbf{I}_{N_t}$ ,  $\hat{\boldsymbol{\varepsilon}}_r = \mathbf{0}_{N_r \times 1}$ ,  $\hat{\boldsymbol{\varepsilon}}_t = \mathbf{0}_{N_t \times 1}$  under the assumption of no array errors.

#### A. Estimation for AoAs, AoDs and Path Gains

In this estimation stage, AoAs, AoDs and path gains  $\{\boldsymbol{\phi}^{(m)}, \boldsymbol{\theta}^{(m)}, \mathbf{Z}^{(m)}\}_{m=1}^M$  are estimated, given the tentative estimates  $\{\hat{\mathbf{C}}_r, \hat{\mathbf{C}}_t, \hat{\mathbf{\Gamma}}_r, \hat{\mathbf{\Gamma}}_t, \hat{\boldsymbol{\varepsilon}}_r, \hat{\boldsymbol{\varepsilon}}_t\}$ , thorough on-grid and off-grid algorithms. Although the on-grid algorithm suffers from quantization errors due to the grid mismatch between the actual angles and the quantized grid points, this method enables the coarse angle search from the grid points over a wide range angle candidates. In contrast, the off-grid algorithm treats angle values as continuous variables, enabling fine estimation without the quantization errors. In the proposed off-grid algorithm, the angle values are finely updated using a gradient descent algorithm, with initial estimates obtained from the on-grid algorithm. Since the angle estimates might converge to a local optima in the neighborhood of the initial values, this method is unable to search over a wide range of the angle domain due to its dependency on the initial values. Particularly, if the off-grid method is applied in the early phase of algorithmic iterations without precise estimates of the array errors, the objective function might not sufficiently decrease, and the angle estimates might converge to a local optima. Therefore, we employ the on-grid method in the early phase of iterations to search for angle estimates over a wide range of angle candidates. In the later phase with accurate estimates of the array errors, the off-grid algorithm is introduced to finely estimate angles with the initial values obtained from the on-grid method.

The switch from the on-grid algorithm to the off-grid algorithm can be performed automatically when the rate of change in the objective function between the  $t$ -th and  $(t+1)$ -th iterations  $\Delta \mathcal{F}$  falls below a threshold value  $\text{Th}_1$  as  $\Delta \mathcal{F} \leq \text{Th}_1$  with  $\Delta \mathcal{F} \triangleq |\mathcal{F}(\boldsymbol{\Omega}_{t+1}) - \mathcal{F}(\boldsymbol{\Omega}_t)| / \mathcal{F}(\boldsymbol{\Omega}_t)$ , where  $\boldsymbol{\Omega}_t$  denotes the estimated parameter set at the  $t$ -th iteration.

Focusing on the AoAs, AoDs and path gains, the objective function in (18) can be separated for each training frame index  $m \in \{1, \dots, M\}$  as  $\mathcal{F} = \sum_{m=1}^M \mathcal{F}^{(m)}(\boldsymbol{\phi}^{(m)}, \boldsymbol{\theta}^{(m)}, \mathbf{Z}^{(m)})$ . Hence, these parameters are estimated independently and in parallel for each training frame  $m$ . In what follows, the on-grid algorithm and the off-grid algorithm are detailed in Section III-A1 and III-A2, respectively.

*1) Coarse Estimation Based on On-Grid Algorithm:* Using the virtual channel representation in (15) with the dictionary matrix  $\tilde{\Psi}_k$  constructed by the angle grids and the tentative estimates for array errors, the objective function for the  $m$ -th training frame in (18) can be approximated as  $\mathcal{F}^{(m)}(\boldsymbol{\phi}^{(m)}, \boldsymbol{\theta}^{(m)}, \tilde{\mathbf{Z}}^{(m)}) \simeq \sum_{k=1}^K \left\| \mathbf{y}_k^{(m)} - \Phi \tilde{\Psi}_k \tilde{\mathbf{z}}_k^{(m)} \right\|_2^2$ , where the path gain vector  $\tilde{\mathbf{z}}_k^{(m)}$  is a sparse vector with common support across all subcarriers  $k \in \{1, \dots, K\}$ , meaning that the path gain matrix  $\tilde{\mathbf{Z}}^{(m)} = [\tilde{\mathbf{z}}_1^{(m)}, \dots, \tilde{\mathbf{z}}_K^{(m)}]$  is a row-sparse matrix because  $\tilde{\mathbf{Z}}^{(m)}$  shares the same angle parameters  $\{\boldsymbol{\phi}^{(m)}, \boldsymbol{\theta}^{(m)}\}$  over all subcarriers. By exploiting

$$\text{minimize}_{\Omega} \mathcal{F}(\Omega) = \sum_{m=1}^M \sum_{p=1}^{N_p} \sum_{k=1}^K \left\| \mathbf{y}_{p,k}^{(m)} - \mathbf{W}_p \mathbf{C}_r \Gamma_r \mathbf{A}_{r,k}(\phi^{(m)}, \epsilon_r) \text{diag}(\mathbf{z}_k^{(m)}) \mathbf{A}_{t,k}^H(\theta^{(m)}, \epsilon_t) \Gamma_t^H \mathbf{C}_t^H \mathbf{F}_p \mathbf{q}_p \right\|_2^2. \quad (18)$$

this sparse property of  $\tilde{\mathbf{Z}}^{(m)}$ , the minimization problem can be reformulated as

$$\text{minimize}_{\tilde{\mathbf{Z}}^{(m)}} \sum_{k=1}^K \left\| \mathbf{y}_k^{(m)} - \Phi \tilde{\Psi}_k \tilde{\mathbf{z}}_k^{(m)} \right\|_2^2 \quad (19a)$$

$$\text{subject to} \quad \left\| \tilde{\mathbf{Z}}^{(m)} \right\|_{2,0} = \hat{L}, \quad (19b)$$

where  $\left\| \tilde{\mathbf{Z}}^{(m)} \right\|_{2,0}$  indicates the number of non-zero rows in  $\tilde{\mathbf{Z}}^{(m)}$ , representing the row sparse nature. In practice, the path gain matrix  $\tilde{\mathbf{Z}}^{(m)}$  is not exact  $L$ -sparse matrix due to energy leakage caused by the quantization errors in the grids. Thus, the number of paths used for the constraint in (19) is set to an overestimated value  $\hat{L} > L$ , considering the propagation environment at the given carrier frequency as in [45].

In the absence of beam squint effects, the dictionary matrix  $\tilde{\Psi}_k$  does not depend on the subcarrier index  $k$ , allowing the minimization problem (19) to be solved using the SOMP algorithm [46] as illustrated in [12]. However, in wideband MIMO systems, it is necessary to consider the subcarrier-wise dictionary  $\tilde{\Psi}_k$  due to beam squint effects. To account for beam squint, the author in [16] solves the problem (19) independently for each subcarrier  $k$ , without taking advantage of the common support property, which leads to performance degradation. Therefore, to account for both the common support sparsity of  $\tilde{\mathbf{Z}}^{(m)}$  and beam squint effects, we employ the DCS-SOMP algorithm [44] to solve the problem (19). By solving the problem (19), the path gain, AoA and AoD estimates,  $\hat{\mathbf{z}}_k^{(m)} \in \mathbb{C}^{\hat{L} \times 1}$ ,  $\hat{\phi}^{(m)} \in \mathbb{R}^{\hat{L} \times 1}$  and  $\hat{\theta}^{(m)} \in \mathbb{R}^{\hat{L} \times 1}$  associated with the non-zero entries of  $\tilde{\mathbf{Z}}^{(m)}$  are obtained.

2) *Fine Estimation Based on Off-Grid Algorithm*: To further refine the estimation accuracy and mitigate the errors resulting from grid mismatch, we introduce an off-grid algorithm utilizing a gradient descent method, inspired by the simultaneous iterative gridless weighted (SIGW) algorithm [45], [47]. The proposed off-grid algorithm, unlike the SIGW algorithm, considers both the beam squint effects and array errors.

Since the objective function in (18), given any  $\phi^{(m)}$  and  $\theta^{(m)}$ , is convex with respect to  $\mathbf{z}_k^{(m)}$ , the path gain estimates can be derived in a closed-form expression as a function of  $\phi^{(m)}$  and  $\theta^{(m)}$ . Using the closed-form solution of  $\mathbf{z}_k^{(m)}$ , the objective function is reformulated as a function of  $\phi^{(m)}$  and  $\theta^{(m)}$ . Then,  $\phi^{(m)}$  and  $\theta^{(m)}$  are updated by a gradient descent manner.

By defining  $\mathbf{t}_{p,k}^{z(m)} \triangleq \mathbf{A}_{t,k}^H(\theta^{(m)}, \hat{\epsilon}_t) \hat{\Gamma}_t^H \hat{\mathbf{C}}_t^H \mathbf{F}_p \mathbf{q}_p \in \mathbb{C}^{\hat{L} \times 1}$  and  $\mathbf{T}_{p,k}^{z(m)} \triangleq \mathbf{W}_p \hat{\mathbf{C}}_r \hat{\Gamma}_r \mathbf{A}_{r,k}(\theta^{(m)}, \hat{\epsilon}_r) \text{diag}(\mathbf{t}_{p,k}^{z(m)}) \in \mathbb{C}^{N_r, \text{RF} \times \hat{L}}$ , the minimization problem for  $\mathbf{z}_k^{(m)}$  can be formulated as

$$\text{minimize}_{\mathbf{z}_k^{(m)}} \sum_{p=1}^{N_p} \left\| \mathbf{y}_{p,k}^{(m)} - \mathbf{T}_{p,k}^{z(m)} \mathbf{z}_k^{(m)} \right\|_2^2. \quad (20)$$

The optimal solution for  $\mathbf{z}_k^{(m)}$  is derived in a closed-form as

$$\hat{\mathbf{z}}_k^{(m)} = \left( \mathbf{T}_k^{z(m)} \right)^\dagger \mathbf{y}_k^{(m)}, \quad (21)$$

where  $\mathbf{T}_k^{z(m)} \triangleq \left[ \mathbf{T}_{1,k}^{z(m)\text{T}}, \dots, \mathbf{T}_{N_p,k}^{z(m)\text{T}} \right]^\text{T} \in \mathbb{C}^{N_r, \text{RF} N_p \times \hat{L}}$  is the stacking matrix that depends on  $\phi^{(m)}$  and  $\theta^{(m)}$ .

Substituting (21) into (20), the objective function for  $\phi^{(m)}$  and  $\theta^{(m)}$  can be reformulated as

$$\mathcal{F}^{(m)}(\phi^{(m)}, \theta^{(m)}) = \sum_{k=1}^K \left\| \mathbf{y}_k^{(m)} - \mathbf{T}_k^{z(m)} \left( \mathbf{T}_k^{z(m)} \right)^\dagger \mathbf{y}_k^{(m)} \right\|_2^2. \quad (22)$$

Based on a gradient decent method, AoAs and AoDs can be updated as

$$\hat{\phi}_{\text{new}}^{(m)} = \hat{\phi}^{(m)} - \eta_\phi \left. \frac{\partial \mathcal{F}^{(m)}}{\partial \phi^{(m)}} \right|_{\phi^{(m)} = \hat{\phi}^{(m)}}, \quad (23)$$

$$\hat{\theta}_{\text{new}}^{(m)} = \hat{\theta}^{(m)} - \eta_\theta \left. \frac{\partial \mathcal{F}^{(m)}}{\partial \theta^{(m)}} \right|_{\theta^{(m)} = \hat{\theta}^{(m)}}, \quad (24)$$

where  $\eta_\phi$  and  $\eta_\theta$  are learning rates, determined by a backtracking line search to ensure that the objective function is non-increasing at every step [43]. The gradients  $\frac{\partial \mathcal{F}^{(m)}}{\partial \phi_l^{(m)}}$  and  $\frac{\partial \mathcal{F}^{(m)}}{\partial \theta_l^{(m)}}$  can be calculated as

$$\frac{\partial \mathcal{F}^{(m)}}{\partial \phi_l^{(m)}} = 2 \sum_{k=1}^K \Re \left[ \hat{z}_{l,k}^{(m)*} \mathbf{d}_{l,k}^{\phi(m)\text{H}} \mathbf{T}_k^{z(m)} \hat{\mathbf{z}}_k^{(m)} - \hat{z}_{l,k}^{(m)} \mathbf{y}_k^{(m)\text{H}} \mathbf{d}_{l,k}^{\phi(m)} \right], \quad (25)$$

$$\frac{\partial \mathcal{F}^{(m)}}{\partial \theta_l^{(m)}} = 2 \sum_{k=1}^K \Re \left[ \hat{z}_{l,k}^{(m)*} \mathbf{d}_{l,k}^{\theta(m)\text{H}} \mathbf{T}_k^{z(m)} \hat{\mathbf{z}}_k^{(m)} - \hat{z}_{l,k}^{(m)} \mathbf{y}_k^{(m)\text{H}} \mathbf{d}_{l,k}^{\theta(m)} \right], \quad (26)$$

where  $\mathbf{d}_{l,k}^{\phi(m)} \in \mathbb{C}^{N_r, \text{RF} N_p \times 1}$  and  $\mathbf{d}_{l,k}^{\theta(m)} \in \mathbb{C}^{N_r, \text{RF} N_p \times 1}$  can be calculated as (27) and (28) in the top of next page, with

$$\mathbf{f}_{l,k}^{\phi(m)} = j \frac{2\pi}{\lambda_c} \left( 1 + \frac{\Delta f_k}{f_c} \right) \left\{ (\mathbf{p}_r + \hat{\epsilon}_r) \odot \mathbf{a}_{r,k}(\hat{\phi}_l^{(m)}, \hat{\epsilon}_r) \right\}, \quad (29)$$

$$\mathbf{f}_{l,k}^{\theta(m)} = j \frac{2\pi}{\lambda_c} \left( 1 + \frac{\Delta f_k}{f_c} \right) \left\{ (\mathbf{p}_t + \hat{\epsilon}_t) \odot \mathbf{a}_{t,k}(\hat{\theta}_l^{(m)}, \hat{\epsilon}_t) \right\}, \quad (30)$$

where  $\mathbf{p}_r \in \mathbb{R}^{N_r \times 1}$  and  $\mathbf{p}_t \in \mathbb{R}^{N_t \times 1}$  are the ideal antenna position vectors defined as  $\mathbf{p}_r = [0, d_r/2, \dots, (N_r - 1)d_r/2]^\text{T}$  and  $\mathbf{p}_t = [0, d_t/2, \dots, (N_t - 1)d_t/2]^\text{T}$ .

## B. Estimation for Mutual Coupling

In this estimation stage, the mutual coupling matrices  $\mathbf{C}_r$  and  $\mathbf{C}_t$  are estimated given the tentative estimates  $\{\hat{\Gamma}_r, \hat{\Gamma}_t, \hat{\epsilon}_r, \hat{\epsilon}_t, \{\hat{\phi}^{(m)}, \theta^{(m)}, \hat{\mathbf{Z}}^{(m)}\}_{m=1}^M\}$ . In what follows, we

$$\mathbf{d}_{l,k}^{\phi(m)} = \left[ \left\{ \left[ \mathbf{t}_{1,k}^{z(m)} \right]_l \mathbf{W}_1 \hat{\mathbf{C}}_r \hat{\mathbf{\Gamma}}_r \mathbf{f}_{l,k}^{\phi(m)} \right\}^T, \dots, \left\{ \left[ \mathbf{t}_{N_p,k}^{z(m)} \right]_l \mathbf{W}_{N_p} \hat{\mathbf{C}}_r \hat{\mathbf{\Gamma}}_r \mathbf{f}_{l,k}^{\phi(m)} \right\}^T \right]^T \quad (27)$$

$$\mathbf{d}_{l,k}^{\theta(m)} = \left[ \left\{ \left( \mathbf{f}_{l,k}^{\phi(m)H} \hat{\mathbf{\Gamma}}_t^H \hat{\mathbf{C}}_t^H \mathbf{F}_1 \mathbf{q}_1 \right) \mathbf{W}_1 \hat{\mathbf{C}}_r \hat{\mathbf{\Gamma}}_r \mathbf{a}_{r,k} \left( \hat{\phi}_l^{(m)}, \hat{\boldsymbol{\varepsilon}}_r \right) \right\}^T, \dots, \left\{ \left( \mathbf{f}_{l,k}^{\phi(m)H} \hat{\mathbf{\Gamma}}_t^H \hat{\mathbf{C}}_t^H \mathbf{F}_{N_p} \mathbf{q}_{N_p} \right) \mathbf{W}_{N_p} \hat{\mathbf{C}}_r \hat{\mathbf{\Gamma}}_r \mathbf{a}_{r,k} \left( \hat{\phi}_l^{(m)}, \hat{\boldsymbol{\varepsilon}}_r \right) \right\}^T \right]^T \quad (28)$$

explain the estimation method for only  $\mathbf{C}_r$ , since the estimation procedures for  $\mathbf{C}_r$  and  $\mathbf{C}_t$  are the same.

The mutual coupling matrix  $\mathbf{C}_r$  is modeled by

$$\mathbf{C}_r = \begin{bmatrix} 1 & c_{r,1,1} & c_{r,1,2} & \cdots & c_{r,1,N_r-1} \\ c_{r,1,1} & 1 & c_{r,2,1} & \cdots & c_{r,2,N_r-2} \\ c_{r,1,2} & c_{r,2,1} & 1 & \cdots & c_{r,3,N_r-3} \\ \vdots & \vdots & \vdots & \ddots & \vdots \\ c_{r,1,N_r-1} & c_{r,2,N_r-2} & c_{r,3,N_r-3} & \cdots & 1 \end{bmatrix}. \quad (31)$$

As described in Section II-A, in the case of a ULA configuration, the mutual coupling matrix  $\mathbf{C}_r$  has a symmetric Toeplitz structure such that  $c_{r,n,i} = c_{r,n',i}$ ,  $n, n', i \in \{1, 2, \dots, N_r-1\}$ . This property reduces the number of parameters to be estimated to  $N_r - 1$ , leading to more efficient estimation for  $\mathbf{C}_r$ . However, antenna spacing errors  $\boldsymbol{\varepsilon}_r$  distort the symmetric Toeplitz structure of the mutual coupling matrix, resulting in a deterioration of estimation performance when utilizing the Toeplitz structure. When the mutual coupling matrix  $\mathbf{C}_r$  is exactly modeled without assuming the Toeplitz structure as written in (31), the number of parameters to be estimated rises to  $N_r(N_r - 1)/2$  because  $\mathbf{C}_r$  is a  $N_r \times N_r$  symmetric matrix. The increase in parameters leads to overfitting to noisy observations and higher computational complexity.

Therefore, to balance the accuracy of modeling and the number of parameters, the proposed method approximately decomposes the mutual coupling matrix  $\mathbf{C}_r$  into a Toeplitz part  $\mathbf{C}_r^{\text{TP}} \in \mathbb{C}^{N_r \times N_r}$  and a non-Toeplitz part  $\mathbf{C}_r^{\text{NTP}} \in \mathbb{C}^{N_r \times N_r}$ . Since the effects of mutual coupling monotonically decrease with distance [26], [48], the coupling coefficients of the first  $q_r$ -antenna elements from the reference antenna, which have significant impact on performance, are modeled using an exact coupling model with a non-Toeplitz structure, while the other coupling coefficients are modeled using a Toeplitz structure to reduce the number of parameters. Then, the mutual coupling matrix  $\mathbf{C}_r$  is approximately decomposed as

$$\mathbf{C}_r \simeq \mathbf{C}_r^{\text{TP}} + \mathbf{C}_r^{\text{NTP}}, \quad (32)$$

with

$$[\mathbf{C}_r^{\text{TP}}]_{n_r, n'_r} = [\mathbf{C}_r^{\text{TP}}]_{n'_r, n_r} = \begin{cases} 1 & (n_r = n'_r) \\ 0 & (n_r < n'_r \leq n_r + q_r) \\ c_{r, n'_r - n_r} & (n_r + q_r < n'_r \leq N_r) \end{cases}, \quad (33)$$

$$[\mathbf{C}_r^{\text{NTP}}]_{n_r, n'_r} = [\mathbf{C}_r^{\text{NTP}}]_{n'_r, n_r} = \begin{cases} 0 & (n_r = n'_r) \\ c_{r, n_r, n'_r} & (n_r < n'_r \leq n_r + q_r) \\ 0 & (n_r + q_r < n'_r \leq N_r) \end{cases}. \quad (34)$$

The mutual coupling matrix in (32) includes unknown parameters  $\mathbf{u}_r \triangleq [\mathbf{u}_{r,0}^T, \mathbf{u}_{r,1}^T, \dots, \mathbf{u}_{r,N_r-1}^T]^T \in \mathbb{C}^{Q_r \times 1}$ , with  $Q_r = N_r - q_r - 1 + q_r(N_r - 1) - q_r(q_r - 1)/2$ , where  $\mathbf{u}_{r,i}$  is defined as

$$\mathbf{u}_{r,i} = \begin{cases} [c_{r,q_r+1}, \dots, c_{r,N_r-1}]^T & (i = 0) \\ [c_{r,i,1}, \dots, c_{r,i,q_r}]^T & (0 < i \leq N_r - q_r) \\ [c_{r,i,1}, \dots, c_{r,i,N_r-i}]^T & (N_r - q_r < i \leq N_r - 1) \end{cases}. \quad (35)$$

The unknown parameters  $\mathbf{u}_{r,0}$  include  $N_r - q_r - 1$  parameters corresponding to Toeplitz part in (33), and  $\mathbf{u}_{r,i}$ , ( $1 \leq i \leq N_r - 1$ ) include  $q_r(N_r - 1) - q_r(q_r - 1)/2$  parameters corresponding to non-Toeplitz part in (34).

Estimating the unknown parameters  $\mathbf{u}_r$  instead of directly estimating  $\mathbf{C}_r$  enables efficient estimation with low computational complexity. Additionally, to account for the property that the coefficients of mutual coupling at close distances have similar values, a regularizer for the estimation of  $\mathbf{u}_r$  is introduced as

$$\sum_{n_r=1}^{N_r} \sum_{i=1}^{\min\{q_r, N_r - n_r\}} |c_{r,n_r,i} - c_{r,n_r+1,i}|^2 = \|\mathbf{S}_r \mathbf{u}_r\|_2^2, \quad (36)$$

where  $\mathbf{S}_r \in \mathbb{R}^{Q_r \times Q_r}$  is the regularization matrix whose entries are 0, 1, or  $-1$ , ensuring that the equation (36) is satisfied.

For any vector  $\mathbf{a} = [a_1, \dots, a_{N_r}]^T \in \mathbb{C}^{N_r \times 1}$ , the following property with respect to  $\mathbf{u}_r$  and  $\mathbf{C}_r$  is hold as

$$\mathbf{C}_r \mathbf{a} = \sum_{i=0}^{N_r-1} \mathbf{Q}_{r,i}(\mathbf{a}) \mathbf{u}_{r,i} + \mathbf{a} = \mathbf{Q}_r(\mathbf{a}) \mathbf{u}_r + \mathbf{a}, \quad (37)$$

with  $\mathbf{Q}_r(\mathbf{a}) = [\mathbf{Q}_{r,0}(\mathbf{a}), \dots, \mathbf{Q}_{r,N_r-1}(\mathbf{a})] \in \mathbb{C}^{N_r \times Q_r}$ , where  $\mathbf{Q}_{r,0}(\mathbf{a}) \in \mathbb{C}^{N_r \times (N_r - q_r - 1)}$  is defined in (38) in the top of next page.

For  $0 < i \leq N_r - q_r$ ,  $\mathbf{Q}_{r,i}(\mathbf{a}) \in \mathbb{C}^{N_r \times q_r}$  is expressed as

$$\mathbf{Q}_{r,i}(\mathbf{a}) = \begin{bmatrix} & & \mathbf{0}_{(i-1) \times q_r} & & \\ a_{i+1} & a_{i+2} & a_{i+3} & \cdots & a_{i+q_r} \\ a_i & 0 & 0 & \cdots & 0 \\ 0 & a_i & 0 & \cdots & 0 \\ 0 & 0 & a_i & \cdots & 0 \\ \vdots & \vdots & \vdots & \ddots & \vdots \\ 0 & 0 & 0 & \cdots & a_i \\ & & \mathbf{0}_{(N_r-i-q_r) \times q_r} & & \end{bmatrix}. \quad (39)$$

$$\mathbf{Q}_{r,0}(\mathbf{a}) = \begin{bmatrix} a_{q_r+2} & a_{q_r+3} & \cdots & a_{N_r-1} & a_{N_r} \\ a_{q_r+3} & a_{q_r+4} & \cdots & a_{N_r} & 0 \\ \vdots & \vdots & \ddots & \vdots & \vdots \\ a_{N_r-1} & a_{N_r} & \cdots & 0 & 0 \\ a_{N_r} & 0 & \cdots & 0 & 0 \end{bmatrix} + \begin{bmatrix} & & & & \mathbf{0}_{(q_r+1) \times (N_r-q_r-1)} \\ & a_1 & 0 & \cdots & 0 & 0 \\ & a_2 & a_1 & \cdots & 0 & 0 \\ \vdots & \vdots & \vdots & \ddots & \vdots & \vdots \\ & a_{N_r-q_r-2} & a_{N_r-q_r-3} & \cdots & a_1 & 0 \\ a_{N_r-q_r-1} & a_{N_r-q_r-2} & \cdots & \cdots & a_2 & a_1 \end{bmatrix}. \quad (38)$$

For  $N_r - q_r < i \leq N_r - 1$ ,  $\mathbf{Q}_{r,i}(\mathbf{a}) \in \mathbb{C}^{N_r \times (N_r-i)}$  is expressed as

$$\mathbf{Q}_{r,i}(\mathbf{a}) = \begin{bmatrix} & & \mathbf{0}_{(i-1) \times (N_r-i)} & & \\ a_{i+1} & a_{i+2} & a_{i+3} & \cdots & a_{N_r} \\ a_i & 0 & 0 & \cdots & 0 \\ 0 & a_i & 0 & \cdots & 0 \\ 0 & 0 & a_i & \cdots & 0 \\ \vdots & \vdots & \vdots & \ddots & 0 \\ 0 & 0 & 0 & \cdots & a_i \end{bmatrix}. \quad (40)$$

By defining  $\mathbf{t}_{p,k}^{\mathbf{c}_r(m)} \triangleq \hat{\mathbf{\Gamma}}_r \mathbf{A}_{r,k}(\hat{\phi}^{(m)}, \hat{\varepsilon}_r) \text{diag}(\hat{\mathbf{z}}_k^{(m)}) \mathbf{A}_{t,k}^H(\hat{\theta}^{(m)}, \hat{\varepsilon}_t) \hat{\mathbf{\Gamma}}_t^H \hat{\mathbf{C}}_t^H \mathbf{F}_p \mathbf{q}_p \in \mathbb{C}^{N_r \times 1}$ , the objective function for  $\mathbf{u}_r$  with the regularizer in (36) is formulated as

$$\begin{aligned} \mathcal{F}(\mathbf{u}_r) &= \sum_{m=1}^M \sum_{p=1}^{N_p} \sum_{k=1}^K \left\| \mathbf{y}_{p,k}^{(m)} - \mathbf{W}_p \mathbf{C}_r \mathbf{t}_{p,k}^{\mathbf{c}_r(m)} \right\|_2^2 + \lambda^{\mathbf{c}_r} \|\mathbf{S}_r \mathbf{u}_r\|_2^2 \\ &\stackrel{(a)}{=} \sum_{m=1}^M \sum_{p=1}^{N_p} \sum_{k=1}^K \left\| \mathbf{y}_{p,k}^{(m)} - \mathbf{W}_p \mathbf{t}_{p,k}^{\mathbf{c}_r(m)} - \mathbf{W}_p \mathbf{Q}_r(\mathbf{t}_{p,k}^{\mathbf{c}_r(m)}) \mathbf{u}_r \right\|_2^2 \\ &\quad + \lambda^{\mathbf{c}_r} \|\mathbf{S}_r \mathbf{u}_r\|_2^2, \end{aligned} \quad (41)$$

where  $\lambda^{\mathbf{c}_r}$  is the penalty coefficient, and the equality in (a) holds using the property (37). Since the regularization term in (41) prevents overfitting caused by the increase in parameters due to the introduction of the non-Toeplitz part, the penalty coefficient is set as  $\lambda^{\mathbf{c}_r} \propto \sigma^2$  to mitigate overfitting in the low SNR region.

The optimal solution of  $\mathbf{u}_r$  is calculated in closed-form as

$$\begin{aligned} \hat{\mathbf{u}}_r &= \left\{ \sum_{m,p,k} \mathbf{Q}_r^H(\mathbf{t}_{p,k}^{\mathbf{c}_r(m)}) \mathbf{W}_p^H \mathbf{W}_p \mathbf{Q}_r(\mathbf{t}_{p,k}^{\mathbf{c}_r(m)}) + \lambda^{\mathbf{c}_r} \mathbf{S}_r^H \mathbf{S}_r \right\}^{-1} \\ &\quad \times \left\{ \sum_{m,p,k} \mathbf{Q}_r^H(\mathbf{t}_{p,k}^{\mathbf{c}_r(m)}) \mathbf{W}_p^H (\mathbf{y}_{p,k}^{(m)} - \mathbf{W}_p \mathbf{t}_{p,k}^{\mathbf{c}_r(m)}) \right\}. \end{aligned} \quad (42)$$

Following a similar procedure in the derivation of (42), the optimal solution for  $\mathbf{u}_t$  can be obtained as

$$\begin{aligned} \hat{\mathbf{u}}_t &= \left\{ \sum_{m,p,k} \mathbf{Q}_t^H(\mathbf{F}_p \mathbf{q}_p) \mathbf{R}_{p,k}^{\mathbf{c}_t(m)H} \mathbf{R}_{p,k}^{\mathbf{c}_t(m)} \mathbf{Q}_t(\mathbf{F}_p \mathbf{q}_p) + \lambda^{\mathbf{c}_t} \mathbf{S}_t^H \mathbf{S}_t \right\}^{-1} \\ &\quad \times \left\{ \sum_{m,p,k} \mathbf{Q}_t^H(\mathbf{F}_p \mathbf{q}_p) \mathbf{R}_{p,k}^{\mathbf{c}_t(m)H} (\mathbf{y}_{p,k}^{(m)} - \mathbf{R}_{p,k}^{\mathbf{c}_t(m)} \mathbf{F}_p \mathbf{q}_p) \right\}, \end{aligned} \quad (43)$$

with  $\mathbf{R}_{p,k}^{\mathbf{c}_t(m)} \triangleq \mathbf{W}_p \hat{\mathbf{C}}_t \hat{\mathbf{\Gamma}}_t \mathbf{A}_{r,k}(\hat{\phi}^{(m)}, \hat{\varepsilon}_r) \text{diag}(\mathbf{z}_k^{(m)}) \mathbf{A}_{t,k}^H(\hat{\theta}^{(m)}, \hat{\varepsilon}_t) \hat{\mathbf{\Gamma}}_t^H \in \mathbb{C}^{N_r, \text{RF} \times N_t}$ . Using the estimates  $\hat{\mathbf{u}}_r$

and  $\hat{\mathbf{u}}_t$ , the mutual coupling matrices  $\hat{\mathbf{C}}_r$  and  $\hat{\mathbf{C}}_t$  can be reconstructed based on the structure in (33) and (34).

In a similar way to the switching mechanism for on-grid and off-grid algorithms described in Section III-A1 and III-A2, the approximate coupling model in (32) is introduced depending on the algorithmic iterations. Due to the low estimation accuracy of each parameter in the early algorithmic iterations, the use of the approximate model in (32) results in poor convergence performance because of an excessive number of parameters in the mutual coupling matrix, which might cause overfitting, particularly with large  $q_r$  and  $q_t$ . To this end, in the early iterations, only the Toeplitz part (i.e.,  $q_r = q_t = 0$ ), without the non-Toeplitz part, is utilized to avoid overfitting induced by inaccurate tentative estimates. When the rate of change in the objective function  $\Delta \mathcal{F}$  falls below a threshold  $\text{Th}_2$  as  $\Delta \mathcal{F} \leq \text{Th}_2$ , the approximate model in (32) is introduced to mitigate model mismatch in the mutual coupling.

### C. Estimation for Gain and Phase Errors

In this stage, we estimate  $\gamma_r$  and  $\gamma_t$  (because of  $\mathbf{\Gamma}_r = \text{diag}(\gamma_r)$ ,  $\mathbf{\Gamma}_t = \text{diag}(\gamma_t)$ ) given the tentative estimates  $\{\hat{\mathbf{C}}_r, \hat{\mathbf{C}}_t, \hat{\varepsilon}_r, \hat{\varepsilon}_t, \{\hat{\phi}^{(m)}, \hat{\theta}^{(m)}, \hat{\mathbf{z}}^{(m)}\}_{m=1}^M\}$ .

Defining  $\mathbf{t}_{p,k}^{\gamma_r(m)} \triangleq \mathbf{A}_{r,k}(\hat{\phi}^{(m)}, \hat{\varepsilon}_r) \text{diag}(\mathbf{z}_k^{(m)}) \mathbf{A}_{t,k}^H(\hat{\theta}^{(m)}, \hat{\varepsilon}_t) \hat{\mathbf{\Gamma}}_t^H \hat{\mathbf{C}}_t^H \mathbf{F}_p \mathbf{q}_p \in \mathbb{C}^{N_r \times 1}$ , the objective function for  $\gamma_r$  can be expressed as

$$\begin{aligned} \mathcal{F}(\gamma_r) &= \sum_{m=1}^M \sum_{p=1}^{N_p} \sum_{k=1}^K \left\| \mathbf{y}_{p,k}^{(m)} - \mathbf{W}_p \hat{\mathbf{C}}_r \text{diag}(\gamma_r) \mathbf{t}_{p,k}^{\gamma_r(m)} \right\|_2^2 \\ &\stackrel{(b)}{=} \sum_{m=1}^M \sum_{p=1}^{N_p} \sum_{k=1}^K \left\| \mathbf{y}_{p,k}^{(m)} - \mathbf{T}_{p,k}^{\gamma_r(m)} \gamma_r \right\|_2^2, \end{aligned} \quad (44)$$

with  $\mathbf{T}_{p,k}^{\gamma_r(m)} \triangleq \mathbf{W}_p \hat{\mathbf{C}}_r \hat{\mathbf{\Gamma}}_r \text{diag}(\mathbf{t}_{p,k}^{\gamma_r(m)}) \in \mathbb{C}^{N_r, \text{RF} \times N_r}$ , where the equality of (b) holds using the property of the diagonal matrix  $\text{diag}(\gamma_r) \mathbf{t}_{p,k}^{\gamma_r(m)} = \text{diag}(\mathbf{t}_{p,k}^{\gamma_r(m)}) \gamma_r$ .

The minimization of the objective function in (44) can be solved in closed form as

$$\hat{\gamma}_r = \left( \sum_{m,p,k} \mathbf{T}_{p,k}^{\gamma_r(m)H} \mathbf{T}_{p,k}^{\gamma_r(m)} \right)^{-1} \left( \sum_{m,p,k} \mathbf{T}_{p,k}^{\gamma_r(m)H} \mathbf{y}_{p,k}^{(m)} \right). \quad (45)$$

Through the same procedure as the derivation of  $\hat{\gamma}_r$  in (45), the gain/phase errors at the UE side,  $\hat{\gamma}_t$  can be obtained as

$$\hat{\gamma}_t = \left( \sum_{m,p,k} \mathbf{T}_{p,k}^{\gamma_t(m)H} \mathbf{T}_{p,k}^{\gamma_t(m)} \right)^{-1} \left( \sum_{m,p,k} \mathbf{T}_{p,k}^{\gamma_t(m)H} \mathbf{y}_{p,k}^{(m)} \right), \quad (46)$$



where  $\mathbf{T}_{p,k}^{\gamma_t(m)} \triangleq \mathbf{W}_p \hat{\mathbf{C}}_r \hat{\mathbf{\Gamma}}_r \mathbf{A}_{r,k}(\hat{\phi}^{(m)}, \hat{\varepsilon}_r) \text{diag}(\hat{\mathbf{z}}_k^{(m)}) \mathbf{A}_{t,k}^H(\hat{\theta}^{(m)}, \hat{\varepsilon}_t) \text{diag}(\mathbf{t}_p^{\gamma_t}) \in \mathbb{C}^{N_r, \text{RF} \times N_r}$ , with  $\mathbf{t}_p^{\gamma_t} = \hat{\mathbf{C}}_t \mathbf{F}_p \mathbf{q}_p \in \mathbb{C}^{N_t \times 1}$ .

#### D. Estimation for Antenna Spacing Errors

In this stage, antenna spacing errors  $\varepsilon_r$  and  $\varepsilon_t$  are estimated by a gradient decent method. Substituting the optimal solution  $\hat{\mathbf{z}}_k^{(m)}$  in (21) into (18), the objective function for  $\varepsilon_r, \varepsilon_t$  is given by

$$\mathcal{F}(\varepsilon_r, \varepsilon_t) = \sum_{m=1}^M \sum_{k=1}^K \left\| \mathbf{y}_k^{(m)} - \mathbf{T}_k^{z(m)} \left( \mathbf{T}_k^{z(m)} \right)^\dagger \mathbf{y}_k^{(m)} \right\|_2^2. \quad (47)$$

Based on a gradient decent method, antenna spacing errors  $\varepsilon_r$  and  $\varepsilon_t$  are updated as

$$\hat{\varepsilon}_{r,\text{new}} = \hat{\varepsilon}_r - \eta_{\varepsilon_r} \left. \frac{\partial \mathcal{F}}{\partial \varepsilon_r} \right|_{\varepsilon_r = \hat{\varepsilon}_r}, \quad (48)$$

$$\hat{\varepsilon}_{t,\text{new}} = \hat{\varepsilon}_t - \eta_{\varepsilon_t} \left. \frac{\partial \mathcal{F}}{\partial \varepsilon_t} \right|_{\varepsilon_t = \hat{\varepsilon}_t}, \quad (49)$$

where  $\eta_{\varepsilon_r}$  and  $\eta_{\varepsilon_t}$  are learning rates, determined by a back-tracking line search [43]. The gradients in (48), (49) are calculated as

$$\frac{\partial \mathcal{F}}{\partial \varepsilon_{r,n_r}} = 2 \sum_{m,k} \Re \left[ \hat{\mathbf{z}}_k^{(m)H} \frac{\partial \mathbf{T}_k^{z(m)H}}{\partial \varepsilon_{r,n_r}} \mathbf{T}_k^{z(m)} \hat{\mathbf{z}}_k^{(m)} - \mathbf{y}_k^{(m)H} \frac{\partial \mathbf{T}_k^{z(m)}}{\partial \varepsilon_{r,n_r}} \hat{\mathbf{z}}_k^{(m)} \right], \quad (50)$$

$$\frac{\partial \mathcal{F}}{\partial \varepsilon_{t,n_t}} = 2 \sum_{m,k} \Re \left[ \hat{\mathbf{z}}_k^{(m)H} \frac{\partial \mathbf{T}_k^{z(m)H}}{\partial \varepsilon_{t,n_t}} \mathbf{T}_k^{z(m)} \hat{\mathbf{z}}_k^{(m)} - \mathbf{y}_k^{(m)H} \frac{\partial \mathbf{T}_k^{z(m)}}{\partial \varepsilon_{t,n_t}} \hat{\mathbf{z}}_k^{(m)} \right], \quad (51)$$

where the gradients of  $\mathbf{T}_{p,k}^{z(m)}$  are calculated as

$$\frac{\partial \mathbf{T}_{p,k}^{z(m)}}{\partial \varepsilon_{r,n_r}} = \hat{\gamma}_{r,n_r} \mathbf{W}_p \left[ \hat{\mathbf{C}}_r \right]_{:,n_r} \mathbf{f}_{n_r,k}^{\varepsilon_r(m)T} \text{diag}(\mathbf{t}_{p,k}^{z(m)}), \quad (52)$$

$$\begin{aligned} \frac{\partial \mathbf{T}_{p,k}^{z(m)}}{\partial \varepsilon_{t,n_t}} &= \mathbf{W}_p \hat{\mathbf{C}}_r \hat{\mathbf{\Gamma}}_r \mathbf{A}_{r,k}(\hat{\phi}^{(m)}, \hat{\varepsilon}_r) \\ &\times \text{diag} \left( \hat{\gamma}_{t,n_t}^* \mathbf{f}_{n_t,k}^{\varepsilon_t(m)*} \left[ \hat{\mathbf{C}}_t \right]_{:,n_t}^H \mathbf{F}_p \mathbf{q}_p \right), \quad (53) \end{aligned}$$

with

$$\mathbf{f}_{n_r,k}^{\varepsilon_r(m)} = \left[ j \frac{2\pi}{\lambda_c} \left\{ 1 + \frac{\Delta f_k}{f_c} \sin(\hat{\phi}^{(m)}) \right\} \right] \odot \left[ \mathbf{A}_{r,k}^T(\hat{\phi}^{(m)}, \hat{\varepsilon}_r) \right]_{:,n_r}, \quad (54)$$

$$\mathbf{f}_{n_t,k}^{\varepsilon_t(m)} = \left[ j \frac{2\pi}{\lambda_c} \left\{ 1 + \frac{\Delta f_k}{f_c} \sin(\hat{\theta}^{(m)}) \right\} \right] \odot \left[ \mathbf{A}_{t,k}^T(\hat{\theta}^{(m)}, \hat{\varepsilon}_t) \right]_{:,n_t}. \quad (55)$$

Finally, from the estimated unknown parameters  $\hat{\mathbf{\Omega}} = \left\{ \hat{\mathbf{C}}_r, \hat{\mathbf{C}}_t, \hat{\mathbf{\Gamma}}_r, \hat{\mathbf{\Gamma}}_t, \hat{\varepsilon}_r, \hat{\varepsilon}_t, \hat{\phi}^{(m)}, \hat{\theta}^{(m)}, \hat{\mathbf{Z}}^{(m)} \right\}_{m=1}^M$ , the channel matrix can be reconstructed as

$$\hat{\mathbf{H}}_k^{(m)} = \hat{\mathbf{C}}_r \hat{\mathbf{\Gamma}}_r \mathbf{A}_{r,k}(\hat{\phi}^{(m)}, \hat{\varepsilon}_r) \text{diag}(\mathbf{z}_k^{(m)}) \mathbf{A}_{t,k}^H(\hat{\theta}^{(m)}, \hat{\varepsilon}_t) \hat{\mathbf{\Gamma}}_t^H \hat{\mathbf{C}}_t^H. \quad (56)$$

The calculation flow of the proposed algorithm is provided in Algorithm 1.

---

#### Algorithm 1 Proposed channel estimation algorithm

---

**Input:**  $T_{\text{iter}}, Th_1, Th_2, q_r, q_t$   
**Output:**  $\{\hat{\mathbf{H}}^{(m)}\}_{m=1}^M$

---

**// Initialization**  
 $\hat{\mathbf{C}}_r = \hat{\mathbf{\Gamma}}_r = \mathbf{I}_{N_r}, \hat{\mathbf{C}}_t = \hat{\mathbf{\Gamma}}_t = \mathbf{I}_{N_t}, \hat{\varepsilon}_r = \mathbf{0}_{N_r}, \hat{\varepsilon}_t = \mathbf{0}_{N_t}$   
**// ML algorithm via alternating optimization**

- 1: **for**  $t = 1, 2, \dots, T_{\text{iter}}$  **do**
- 2:   **if**  $\Delta \mathcal{F} > Th_1$  **then**
- 3:     Update  $\hat{\mathbf{z}}_k^{(m)}, \hat{\phi}^{(m)}$  and  $\hat{\theta}^{(m)}$  by solving (19) via DCS-SOMP [44]
- 4:     Update  $\hat{\mathbf{C}}_r$  and  $\hat{\mathbf{C}}_t$  from (42) and (43) with  $q_t = q_r = 0$
- 5:   **else**
- 6:     Update  $\hat{\mathbf{z}}_k^{(m)}, \hat{\phi}^{(m)}$  and  $\hat{\theta}^{(m)}$  by the gradient decent from (21), (23) and (24)
- 7:     **if**  $\Delta \mathcal{F} > Th_2$  **then**
- 8:       Update  $\hat{\mathbf{C}}_r$  and  $\hat{\mathbf{C}}_t$  from (42) and (43) with  $q_t = q_r = 0$
- 9:     **else**
- 10:       Update  $\hat{\mathbf{C}}_r$  and  $\hat{\mathbf{C}}_t$  from (42) and (43) with  $q_t$  and  $q_r$
- 11:     **end if**
- 12:   **end if**
- 13:   Update  $\hat{\mathbf{\Gamma}}_r$  and  $\hat{\mathbf{\Gamma}}_t$  from (45) and (46)
- 14:   Update  $\hat{\varepsilon}_r$  and  $\hat{\varepsilon}_t$  from (48) and (49)
- 15: **end for**

**// Channel estimation**  
 16: Calculate  $\hat{\mathbf{H}}^{(m)}$  from (56)

---

#### E. Complexity Analysis

Computational complexity of the proposed algorithm is evaluated in terms of the number of complex multiplications as floating operations (FLOPs). The proposed method, as shown in Algorithm 1, alternately estimates each parameter  $\{\mathbf{C}_r, \mathbf{C}_t, \mathbf{\Gamma}_r, \mathbf{\Gamma}_t, \varepsilon_r, \varepsilon_t, \{\phi^{(m)}, \theta^{(m)}, \mathbf{Z}^{(m)}\}_{m=1}^M\}$ . The FLOPs for estimating each parameter per iteration are provided in Table I, where the complexity of estimating  $\{\phi^{(m)}, \theta^{(m)}, \mathbf{Z}^{(m)}\}$  using both the on-grid DCS-SOMP [44] and the off-grid method from (21), (23) and (24) is presented since the estimation methods are switched from the on-grid method to the on-grid method based on the rate of change in the objective function.

In the case of using the exact mutual coupling model in (31) (i.e., setting  $q_r = N_r - 1$  and  $q_t = N_t - 1$  in (35)), the dominant complexity in the entire algorithm is  $\mathcal{O}(MKN_p N_r, \text{RF}(N_r^4 + N_t^4) + N_r^6 + N_t^6)$  for estimating  $\mathbf{C}_r$  and  $\mathbf{C}_t$  because equations (42), (43) require matrix multiplications and an inverse operations with size  $Q_r \times Q_r$  and  $Q_t \times Q_t$  matrices, where  $Q_r = q_r(N_r - 1) - q_r(q_r - 1)/2$  and  $Q_t = q_t(N_t - 1) - q_t(q_t - 1)/2$ . On the other hand, the proposed algorithm can reduce the complexity by selecting small values for  $q_r$  and  $q_t$  (e.g.,  $q_r = q_t = 2$  in the simulation of Section IV) by considering the property of mutual coupling. When  $q_r = q_t = 0$ , meaning that the mutual coupling matrix is assumed to be modeled as a Toeplitz matrix,

TABLE I: Computational complexity of the proposed algorithm

| Estimation parameters                                       | FLOPs  |
|---|--|
| $\mathbf{z}, \phi, \boldsymbol{\theta}$ in (21), (25), (26) | $\mathcal{O}\left(MKN_p(N_r^2(N_{r,\text{RF}} + \hat{L}) + N_t^2\hat{L})\right)$ |
| $\mathbf{z}, \phi, \boldsymbol{\theta}$ (DCS-SOMP [44])     | $\mathcal{O}\left(MKN_pN_{r,\text{RF}}G_\theta G_\phi + MK\hat{L}^4\right)$      |
| $\mathbf{C}_r, \mathbf{C}_t$ in (42), (43)                  | $\mathcal{O}\left(MKN_pN_{r,\text{RF}}(Q_r^2 + Q_t^2) + Q_r^3 + Q_t^3\right)$    |
| $\Gamma_r, \Gamma_t$ in (45), (46)                          | $\mathcal{O}\left(MKN_pN_{r,\text{RF}}(N_r^2 + N_t^2) + N_r^3 + N_t^3\right)$    |
| $\varepsilon_r, \varepsilon_t$ in (50), (51)                | $\mathcal{O}\left(MKN_pN_{r,\text{RF}}N_r(N_r + \hat{L})\right)$                 |

Note:  $Q_r = q_r(N_r - 1) - q_r(q_r - 1)/2$ ,  $Q_t = q_t(N_t - 1) - q_t(q_t - 1)/2$ .

TABLE II: Simulation parameters

| Parameter                 | Variable                           | Value                                |
|---------------------------|------------------------------------|--------------------------------------|
| Carrier frequency         | $f_c$                              | 50 GHz                               |
| Bandwidth                 | $B$                                | 2.5 GHz                              |
| Num. of subcarrier        | $K$                                | 64                                   |
| Num. of antennas          | $N_r, N_t$                         | 32, 8                                |
| Num. of RF chains         | $N_{r,\text{RF}}, N_{t,\text{RF}}$ | 2, 2                                 |
| Num. of training frames   | $M$                                | 2, 5                                 |
| Num. of pilots            | $N_p$                              | 32, 50                               |
| Num. of quantization bits | $N_Q$                              | 2                                    |
| Num. of paths             | $L$                                | 6                                    |
| Num. of estimated paths   | $\hat{L}$                          | 12                                   |
| Num. of grids             | $G_\theta, G_\phi$                 | 64, 16                               |
| Ideal antenna spacing     | $d_r, d_t$                         | $\lambda_c/2$                        |
| Num. of iterations        | $T_{\text{iter}}$                  | 250                                  |
| Coupling parameters       | $q_r, q_t$                         | 2, 2                                 |
| Threshold parameters      | $\text{Th}_1, \text{Th}_2$         | $1 \times 10^{-3}, 1 \times 10^{-3}$ |
| Penalty coefficients      | $\lambda^{c_r}, \lambda^{c_t}$     | $\text{SNR}^{-1} \times 10^2$        |

the complexity can be minimized. However the estimation performance significantly degrades due to the modeling errors. The estimation performance and complexity for various values of  $q_r$  and  $q_t$  will be provided in the following simulation results in Section IV.

## IV. SIMULATION RESULTS

### A. Simulation Setup

This section evaluates the performance of the proposed channel estimation algorithm under the simulation parameters provided in Table II.

The channels defined in (1) are generated by the composition of total  $L = 6$  paths, where path gain  $\alpha_l$  is generated as  $\alpha_l \sim \mathcal{CN}(0, 1/L)$ , AoA  $\phi_l$  and AoD  $\theta_l$  are uniformly distributed in  $[-\pi, \pi)$ , and delay  $\tau_l$  is uniformly distributed in  $[0, (N_{\text{tap}} - 1)/B]$ , as in [12], [16], [18], where  $N_{\text{tap}} = 16$  is the number of delay taps.

The array errors are generated by the following models in [16]–[19], [48]. The gain and phase errors are generated as  $g_{r,n_r}, g_{t,n_t} \sim \mathcal{N}(1, 0.05^2)$  and  $\nu_{r,n_r}, \nu_{t,n_t} \sim \mathcal{N}(0, (20\pi/180)^2)$ , and the antenna spacing errors are generated as  $\varepsilon_{r,n_r}, \varepsilon_{t,n_t} \sim \mathcal{U}(-0.1\lambda_c, 0.1\lambda_c)$ . Since effects of the mutual coupling decrease with distance from a reference antenna [26], [48], the coefficient of the mutual coupling can be modeled as a function of distance as  $c(\tilde{r}) = \frac{c_0}{\tilde{r}} e^{-j(\tilde{r}-1)\pi/8}$ , where  $\tilde{r}$  is the distance normalized by half wavelength  $\lambda_c/2$ , and  $c_0$  is the coupling coefficient at  $\tilde{r} = 1$ , set to  $c_0 = 0.4e^{j\frac{\pi}{8}}$  in the simulation.

The channel estimation performance is evaluated by normalized mean-squared error (NMSE) under various signal-to-

noise ratio (SNR). SNR and NMSE are defined as  $\text{SNR} \triangleq \frac{P_s}{\sigma^2}$  and

$$\text{NMSE}(\mathbf{H}) \triangleq \mathbb{E} \left[ \frac{\|\mathbf{H} - \hat{\mathbf{H}}\|_F^2}{\|\mathbf{H}\|_F^2} \right], \quad (57)$$

where  $\mathbf{H}$  and  $\hat{\mathbf{H}}$  are a true channel and estimated channel matrices. To assess the pilot overhead for channel estimation, the compression ratio  $\nu \triangleq \frac{N_{r,\text{RF}}N_p}{N_rN_t}$  is defined as the ratio between the number of observations and the number of unknown parameters in the channel matrix. If the compression ratio  $\nu$  is less than 1, the measurement equation in (13) becomes an underdetermined system. In the simulations, the number of pilots  $N_p$  ranges from 32 to 160, corresponding to compression ratios between 0.25 and 1.25.

To assess the effectiveness of the proposed algorithm, the following methods are used as benchmarks.

- 1) SOMP w/ CoDL [16]: a dictionary learning-based channel estimation method, where the dictionary matrix  $\tilde{\Psi}$  in (15) is directly updated with training pilots to compensate for the array errors.
- 2) DA-OMP-BS w/ DLHWBS [18]: a dictionary learning-based channel estimation method, where the dictionary matrix  $\tilde{\Psi}$  in (15) is decomposed into two dictionaries at the transmitter and receiver sides, which are alternately updated with training pilots to compensate for the array errors.
- 3) Prop. (w/o switch,  $q_r = q_t = 0$ ): the proposed method under the assumption that the mutual coupling has Toeplitz structure (i.e.,  $q_r = q_t = 0$ ). This method does not utilize the switching from the on-grid to off-grid algorithms (i.e.,  $\text{Th}_1 \rightarrow \infty$ ). The initial estimates  $\{\hat{\phi}^{(m)}, \hat{\theta}^{(m)}\}$  are generated by DCS-SOMP [44].
- 4) Prop. ( $q_r = q_t = 0$ ): the proposed method under Toeplitz assumption with the switching from the on-grid to off-grid algorithms.
- 5) Prop. ( $q_r = N_r - 1, q_t = N_t - 1$ ): the proposed method under the exact mutual coupling model without exploiting Toeplitz structure.
- 6) Prop. ( $q_r = q_t = 2$ ): the proposed method.
- 7) Genie-aided: the proposed method with perfect knowledge of all array errors.

In conventional dictionary learning methods [16], [18], it is assumed that the dictionary learning for array error calibration is performed offline with a large number of training pilots (e.g.,  $M = 100$  and  $N_p = 500$  in [16], [18]), after which online channel estimation with a small number of pilots is performed using the updated dictionary matrix. However, the offline calibration is ineffective since the array errors fluctuate due to various time-varying factors [20]–[31]. Thus, this simulation assumes that calibration and channel estimation are performed simultaneously without offline calibration, using a small number of pilots and training frames, provided in Table II.

### B. Channel Estimation Performance

Fig. 1a and Fig. 1b show the NMSE performance against SNR and the number pilots  $N_p$  under the number of training frames  $M = 5$ , where the compression ratio  $\nu$  varies from

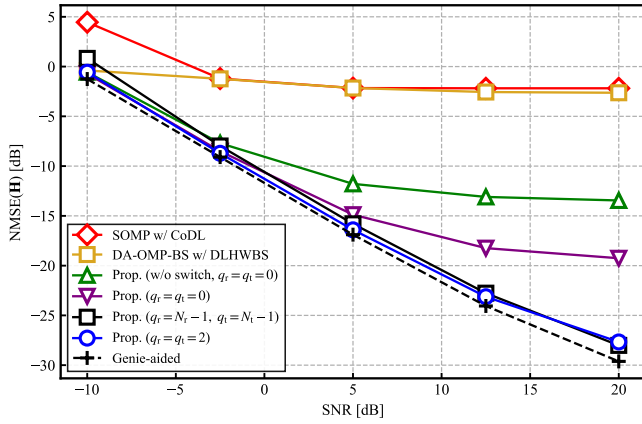
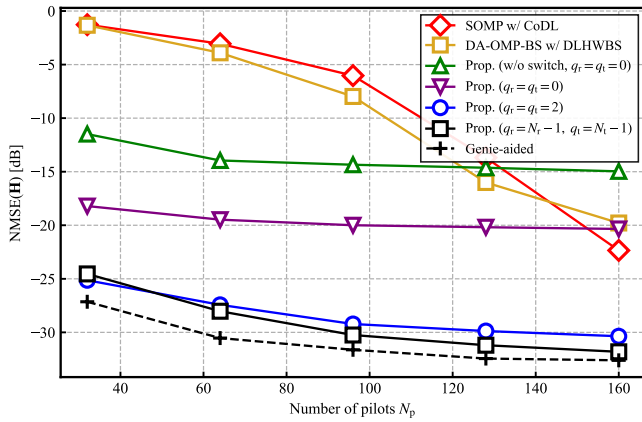

 (a) NMSE( $\mathbf{H}$ ) versus SNR with  $N_p = 50$  (compression ratio  $\nu = 0.391$ ).

 (b) NMSE( $\mathbf{H}$ ) versus the number of pilots  $N_p$  with SNR = 20 dB. The compression ratio  $\nu$  varies from 0.25 to 1.25.

 Fig. 1: NMSE performance with  $M = 5$ .

0.25 to 1.25. As depicted in these figures, the conventional methods, SOMP w/ CoDL and DA-OMP-BS w/ DLHWBS, fail to improve channel estimation performance, especially in a small number of pilots, because these methods estimate the dictionary matrix, which includes a large number of unknown parameters. Although the channel estimation performance improves as the number of pilots increases, it causes significant pilot overhead issues. On the other hand, the proposed method enhances channel estimation performance compared to conventional methods, even in the small pilot region, because the proposed method decomposes the dictionary matrix into multiple channel components, including array errors, based on the array model, and estimates a small number of parameters. Comparing Prop. (w/o switch,  $q_r = q_t = 0$ ) and Prop. ( $q_r = q_t = 0$ ), it can be seen that the switching mechanism from the on-grid to off-grid method significantly improves estimation performance, particularly in the high SNR region, owing to avoiding convergence to the local optima in early algorithmic iterations. As seen from the result of Prop. (w/o switch,  $q_r = q_t = 0$ ) that relies on the Toeplitz structure, the Toeplitz assumption causes the NMSE performance to saturate even with increasing SNR. There is a substantial performance gap of about 9 dB at SNR = 20 dB compared to the

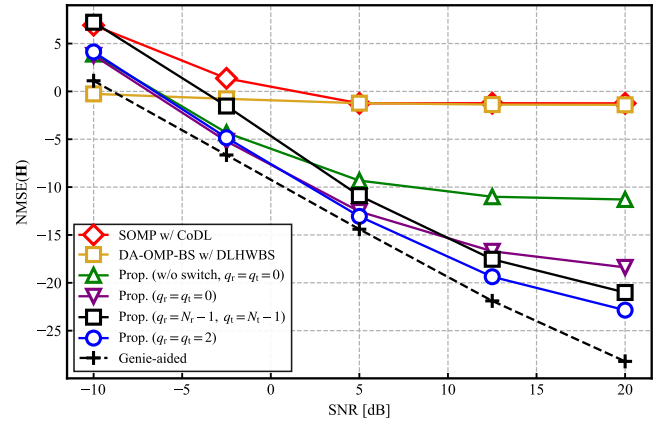
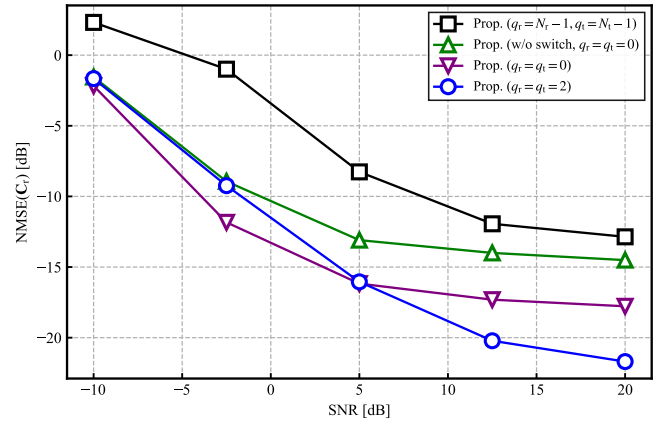
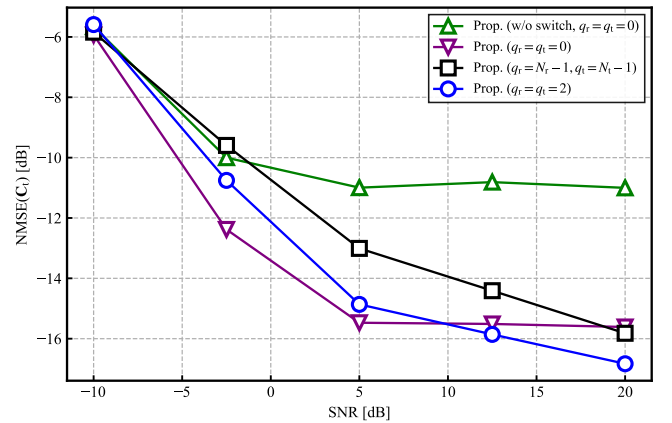

 (a) NMSE( $\mathbf{H}$ ) versus SNR.

 (b) NMSE( $\mathbf{C}_r$ ) versus SNR.

 (c) NMSE( $\mathbf{C}_t$ ) versus SNR.

 Fig. 2: NMSE performance under limited observations for channel estimation with  $M = 2$  and  $N_p = 32$  (compression ratio  $\nu = 0.25$ ).

Genie-aided case, due to the mismatch in the mutual coupling model under the Toeplitz assumption, which is caused by antenna spacing errors. By contrast, the NMSE performance of Prop. ( $q_r = q_t = 2$ ) improves with increasing SNR and approaches the Genie-aided case, owing to the introduction of the approximate mutual coupling model in (32), where the mutual coupling matrix is decomposed into a Toeplitz part and a non-Toeplitz part to account for coupling effects. Thus, the

comparison of Prop. ( $q_r = q_t = 0$ ) and Prop. ( $q_r = q_t = 2$ ) reveals the performance gain resulting from the incorporation of the approximate mutual coupling model in (32). In addition, the proposed method can achieve similar performance to Prop. ( $q_r = N_r - 1, q_t = N_t - 1$ ), which relies on the exact mutual coupling model without Toeplitz structure, despite achieving complexity reduction by adopting a smaller value of  $q_r$  and  $q_t$ . Focusing on the low SNR and small pilot regions, the performance of the proposed method with the approximate coupling model is slightly superior to that of the exact coupling model.

To further investigate the effective range of the proposed method, we offer additional results in scenarios where only limited training observations are available for channel estimation. Fig. 2 shows the NMSE performance against SNR with the number of training frames  $M = 2$  and the number of pilots  $N_p = 32$ , corresponding to the compression ratio  $\nu = 0.25$ . As shown in Fig. 2a, NMSE performance of Prop. ( $q_r = N_r - 1, q_t = N_t - 1$ ) with the exact coupling model deteriorates in the low SNR region compared to Prop. ( $q_r = q_t = 2$ ) with the approximate coupling model. This performance gap is attributed to the significant increase in the number of unknown parameters associated with the mutual coupling matrix  $\mathbf{C}_r$ . The number of unknown parameters with  $q_r = 2$  is  $Q_r = 90$ , but it rises to  $Q_r = 496$  when  $q_r = N_r - 1$ . This increase in the number of parameters not only raises computational complexity but also leads to overfitting to noisy observations, particularly in the low SNR region. Fig. 2b and Fig. 2c shows the estimation performance for the mutual coupling matrices  $\mathbf{C}_r$  and  $\mathbf{C}_t$  against SNR. Although Prop. ( $q_r = N_r - 1, q_t = N_t - 1$ ) exploits the exact mutual coupling model, the estimation performance degrades due to the excessive increase in the number of unknown parameters, leading to overfitting. In contrast, Prop. ( $q_r = q_t = 2$ ) delivers superior performance because part of the mutual coupling matrix is treated with the exact model, while the other part is modeled using a Toeplitz structure with fewer parameters.

To clarify the performance gains from modifying the coupling model and introducing the switching mechanism for the on-grid and off-grid methods, Fig. 3 illustrates the NMSE performance over algorithmic iterations with SNR = 20 dB,  $M = 5$  and  $N_p = 50$ . In this figure, the dashed lines represent the non-averaged performance for a single channel realization, whereas the solid lines represent the averaged performance obtained through Monte Carlo simulations. As seen from Prop. (w/o switch,  $q_r = q_t = 0$ ), which use only the off-grid method without the switching mechanism, the performance converges to a low NMSE of approximately  $-13$  dB. Employing the off-grid algorithm based on gradient descent during the early iterations might lead to convergence to local optima with low NMSE, because the estimation accuracy of the array errors is insufficient in the early iterations. On the other hand, by applying the on-grid method in the early iterations and switching to the off-grid method after convergence, NMSE performance improvement of about 5 dB can be observed from the result of Prop. ( $q_r = q_t = 0$ ). Furthermore, introducing the approximate mutual coupling model in (32) after the convergence of the on-grid method results in performance

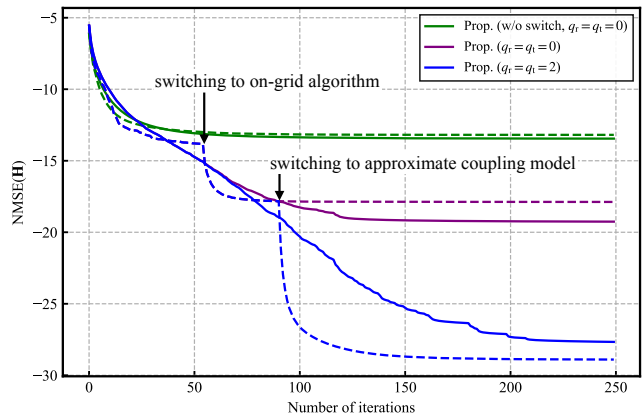


Fig. 3: NMSE(H) versus the number of algorithmic iterations with SNR = 20 dB,  $M = 5$  and  $N_p = 50$  (compression ratio is  $\nu = 0.391$ ). Dashed lines depict one-shot performance of channel estimation given a single channel realization, whereas solid lines indicate averaged performance calculated by Monte Carlo simulations.

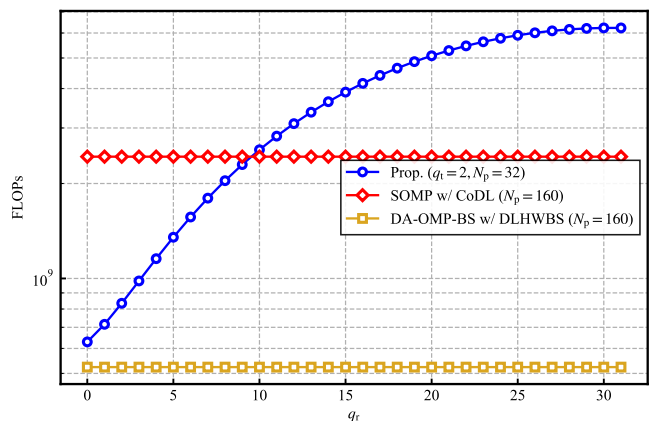


Fig. 4: FLOPs versus  $q_r$  with  $M = 5$  and  $q_t = 2$ . The number of pilots is set to  $N_p = 32$  for the proposed method and  $N_p = 160$  for the conventional methods to evaluate the complexity in achieving same NMSE level.

enhancement of about 8.4 dB, as seen in Prop. ( $q_r = q_t = 2$ ).

### C. Computational Complexity

Fig. 4 shows the computational complexity, evaluated by the number of complex multiplications per iteration as FLOPs, as a function of  $q_r$ . To assess the computational complexity in achieving the same NMSE level, the number of pilots is set to  $N_p = 32$  for the proposed method and  $N_p = 160$  for the conventional methods, based on the result in Fig. 1b. As shown in the figure, the complexity of the proposed method grows monotonically with  $q_r$  due to the increasing number of unknown parameters to be estimated. The results from Fig. 4 and Fig. 2a indicate that setting  $q_r$  to a large value is unfavorable in terms of both high computational burden and a deterioration in channel estimation performance in low SNR regions. When  $q_r$  is set to a small value, the complexity of the proposed method is comparable to that of SOMP w/ CoDL and higher than that of DA-OMP-BS w/ DLHWBS. While the complexity of the proposed method with  $q_r = 2$  is approximately 1.59 times higher than that of DA-OMP-

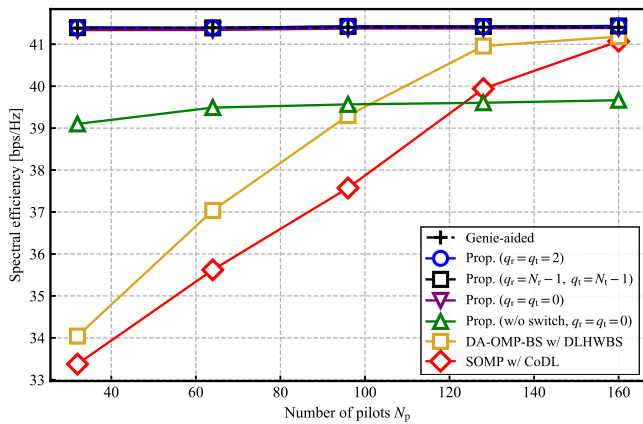


Fig. 5: Spectral efficiency versus the number of pilots  $N_p$  with  $M = 5$  and SNR = 20 dB.

BS w/ DLHWBS, the pilot overhead can be reduced to 20%. Therefore, the proposed method can significantly reduce pilot overhead at the cost of a slight increase in computational complexity.

#### D. Spectral Efficiency Performance

The channel estimation performance is also evaluated by spectral efficiency (SE) using estimated CSI. SE is computed under the assumption of a full digital precoder and combiner as in [12], [16], [18]. The precoder and combiner are designed as the left and right singular vectors corresponding to the dominant  $N_s$  singular values of the estimated channel matrix. The effective channel matrix at the  $k$ -th subcarrier after precoding and combining is expressed as  $\mathbf{H}_{\text{eff},k} \triangleq [\hat{\mathbf{U}}_k]^H \mathbf{H}_k [\hat{\mathbf{V}}_k]_{:,1:N_s}$ , where  $\hat{\mathbf{U}}_k \in \mathbb{C}^{N_r \times N_r}$  and  $\hat{\mathbf{V}}_k \in \mathbb{C}^{N_t \times N_t}$  are the left and right singular vectors of the estimated channel matrix  $\hat{\mathbf{H}}_k$ . Then, the SE is given by

$$\text{SE} = \frac{1}{K} \sum_{k=1}^K \sum_{n_s=1}^{N_s} \log_2 \left( 1 + \frac{\text{SNR}}{N_s} \lambda_{n_s}^2(\mathbf{H}_{\text{eff},k}) \right), \quad (58)$$

where  $\lambda_{n_s}(\mathbf{H}_{\text{eff},k})$  is the singular value of the effective channel matrix  $\mathbf{H}_{\text{eff},k}$ . Fig. 5 shows SE against the number of pilots  $N_p$  with the number of training frames  $M = 5$  and SNR = 20 dB. The conventional methods, SOMP w/ CoDL and DA-OMP-BS w/ DLHWBS, experience significant SE degradation when the number of pilots is small, due to severe channel estimation performance as seen in Fig. 1b. The proposed methods approach the performance of the Genie-aided case even with a limited number of pilots, indicating a reduction in pilot overhead.

#### V. CONCLUSION

In this paper, we proposed a channel estimation method for hybrid wideband MIMO systems affected by array errors and beam squint effects. Due to array deformation from thermal effects and dynamic motion, array errors, such as mutual coupling, gain/phase errors and antenna spacing errors, change over time. To calibrate these array errors online with small pilot overhead, the proposed method reduces the number of unknown parameters by explicitly decomposing the array

response matrices into primary parameters, including AoAs, AoDs, path gains and array errors. These parameters are estimated iteratively via an alternating minimization technique, where an on-grid algorithm and an off-grid algorithm are switched depending on the estimation accuracy of array errors to avoid convergence to a local optima in the early iterations. Furthermore, the mutual coupling matrix is approximately decomposed into a Toeplitz part and a non-Toeplitz part, focusing on a characteristic that coupling effects decrease with distance. The approximate decomposition reduces the number of parameters, resulting in both reduced computational complexity and alleviated overfitting to noisy observations, especially with a small number of training pilots in low SNR regions. Numerical simulations revealed that the channel estimation performance of the proposed method outperforms the conventional methods and approaches the Genie-aided case with perfect knowledge of array errors, even with small pilot overhead.

#### REFERENCES

- [1] K. Arai and K. Ishibashi, "Self-Calibration for Channel Estimation in Hybrid Millimeter-Wave MIMO Systems," in *Proc. IEEE 98th Veh. Technol. Conf. (VTC-Fall)*, 2023, pp. 1–5.
- [2] H. Tataria, M. Shafi, A. F. Molisch, M. Dohler, H. Sjöland, and F. Tufvesson, "6G wireless systems: Vision, requirements, challenges, insights, and opportunities," *Proc. IEEE*, vol. 109, no. 7, pp. 1166–1199, 2021.
- [3] M. Giordani, M. Polese, M. Mezzavilla, S. Rangan, and M. Zorzi, "Toward 6G networks: use cases and technologies," *IEEE Commun. Mag.*, vol. 58, no. 3, pp. 55–61, 2020.
- [4] T. S. Rappaport, G. R. MacCartney, M. K. Samimi, and S. Sun, "Wideband millimeter-wave propagation measurements and channel models for future wireless communication system design," *IEEE Trans. on Commun.*, vol. 63, no. 9, pp. 3029–3056, 2015.
- [5] S. Tarboush, H. Sarrideen, H. Chen, M. H. Loukil, H. Jemaa, M.-S. Alouini, and T. Y. Al-Naffouri, "TeraMIMO: A channel simulator for wideband ultra-massive MIMO terahertz communications," *IEEE Trans. Veh. Technol.*, vol. 70, no. 12, pp. 12325–12341, 2021.
- [6] R. W. Heath, N. Gonzalez-Prelcic, S. Rangan, W. Roh, and A. M. Sayeed, "An overview of signal processing techniques for millimeter wave mimo systems," *IEEE J. Sel. Topics Signal Process.*, vol. 10, no. 3, pp. 436–453, 2016.
- [7] I. Ahmed, H. Khammari, A. Shahid, A. Musa, K. S. Kim, E. De Poorter, and I. Moerman, "A survey on hybrid beamforming techniques in 5G: Architecture and system model perspectives," *IEEE Commun. Surveys Tuts.*, vol. 20, no. 4, pp. 3060–3097, 2018.
- [8] X. Yu, J.-C. Shen, J. Zhang, and K. B. Letaief, "Alternating minimization algorithms for hybrid precoding in millimeter wave MIMO systems," *IEEE J. Sel. Topics Signal Process.*, vol. 10, no. 3, pp. 485–500, 2016.
- [9] S. Srivastava, A. Tripathi, N. Varshney, A. K. Jagannatham, and L. Hanzo, "Hybrid transceiver design for tera-hertz MIMO systems relying on Bayesian learning aided sparse channel estimation," *IEEE Trans. on Wireless Commun.*, vol. 22, no. 4, pp. 2231–2245, 2023.
- [10] F. Sohrabi and W. Yu, "Hybrid digital and analog beamforming design for large-scale antenna arrays," *IEEE J. Sel. Topics Signal Process.*, vol. 10, no. 3, pp. 501–513, 2016.
- [11] X. Ge, W. Shen, C. Xing, L. Zhao, and J. An, "Training beam design for channel estimation in hybrid mmwave MIMO systems," *IEEE Trans. on Wireless Commun.*, vol. 21, no. 9, pp. 7121–7134, 2022.
- [12] J. Rodríguez-Fernández, N. González-Prelcic, K. Venugopal, and R. W. Heath, "Frequency-domain compressive channel estimation for frequency-selective hybrid millimeter wave MIMO systems," *IEEE Trans. Wireless Commun.*, vol. 17, no. 5, pp. 2946–2960, 2018.
- [13] S. Uchimura, K. Ishibashi, H. Iimori, P. V. Klaine, and S. Malomsoy, "Efficient channel tracking based on compressive sensing for OFDM millimeter-wave systems," *IEEE Trans. Veh. Technol.*, vol. 73, no. 8, pp. 11411–11426, 2024.

- [14] K. Furuta, T. Takahashi, and H. Ochiai, "Sparse Bayesian learning using complex t-prior for beam-domain massive MIMO channel estimation," *IEEE Open Journal of the Communications Society*, vol. 5, pp. 5905–5920, 2024.
- [15] M. Eberhardt, P. Eschlwech, and E. Biebl, "Investigations on antenna array calibration algorithms for direction-of-arrival estimation," *Adv. Radio Sci.*, vol. 14, pp. 181–190, 2016.
- [16] H. Xie and N. González-Prelcic, "Dictionary learning for channel estimation in hybrid frequency-selective mmWave MIMO systems," *IEEE Trans. Wireless Commun.*, vol. 19, no. 11, pp. 7407–7422, 2020.
- [17] P. Maity, S. Srivastava, S. Khatri, and A. K. Jagannatham, "Dictionary-learning (DL)-based sparse CSI estimation in multiuser terahertz (THz) hybrid MIMO systems under hardware impairments and beam-Squint effect," *IEEE Access*, vol. 10, pp. 113 699–113 714, 2022.
- [18] H. Xie, J. Palacios, and N. González-Prelcic, "Hybrid mmwave MIMO systems under hardware impairments and beam squint: channel model and dictionary learning-aided configuration," *IEEE Trans. Wireless Commun.*, vol. 22, no. 10, pp. 6898–6913, 2023.
- [19] P. Maity, S. Khatri, S. Srivastava, and A. K. Jagannatham, "Dictionary learning (DL)-based sparse cascaded channel estimation in IRS-assisted terahertz MU-SIMO systems with hardware impairments," in *Proc. IEEE Stat. Signal Process. Workshop (SSP)*, 2023, pp. 606–610.
- [20] H. Liu, W. Wang, D. Tang, L. Zhang, Y. Wang, and E. Miao, "Thermal deformation modeling for phased array antenna compensation control," *Sensors*, vol. 22, no. 6, 2022.
- [21] P. Xu, Y. Wang, X. Xu, L. Wang, Z. Wang, K. Yu, W. Wu, M. Wang, G. Leng, D. Ge, X. Ma, and C. Wang, "Structural-electromagnetic-thermal coupling technology for active phased array antenna," *Int. J. Antennas Propag.*, vol. 2023, no. 1, p. 2843443, 2023.
- [22] K. Cao, C. Jin, B. Zhang, Q. Lv, and F. Lu, "Beam stabilization of deformed conformal array antenna based on physical- method -driven deep learning," *IEEE Trans. Antennas Propag.*, vol. 71, no. 5, pp. 4115–4127, 2023.
- [23] C. Wang, Y. Wang, Y. Chen, W. Gao, Q. Xu, Z. Wang, J. Liu, C. Zhou, W. Xu, and J. Zhong, "Coupling model and electronic compensation of antenna-radome system for hypersonic vehicle with effect of high-temperature ablation," *IEEE Trans. Antennas Propag.*, vol. 68, no. 3, pp. 2340–2355, 2020.
- [24] T. Takahashi, N. Nakamoto, M. Ohtsuka, T. Aoki, Y. Konishi, and M. Yajima, "A simple on-board calibration method and its accuracy for mechanical distortions of satellite phased array antennas," in *3rd European Conf. on Antennas Propag.*, 2009, pp. 1573–1577.
- [25] L. Song and Y. Rahmat-Samii, "A systematic investigation of rectangular patch antenna bending effects for wearable applications," *IEEE Trans. Antennas Propag.*, vol. 66, no. 5, pp. 2219–2228, 2018.
- [26] A. Fikes, O. S. Mizrahi, and A. Hajimiri, "A framework for array shape reconstruction through mutual coupling," *IEEE Trans. Microw. Theory Techn.*, vol. 69, no. 10, pp. 4422–4436, 2021.
- [27] L. Zhu, W. Ma, and R. Zhang, "Movable antennas for wireless communication: opportunities and challenges," *IEEE Commun. Mag.*, vol. 62, no. 6, pp. 114–120, 2024.
- [28] W. Ma, L. Zhu, and R. Zhang, "Compressed sensing based channel estimation for movable antenna communications," *IEEE Commun. Lett.*, vol. 27, no. 10, pp. 2747–2751, 2023.
- [29] K.-K. Wong, A. Shojaefard, K.-F. Tong, and Y. Zhang, "Fluid antenna systems," *IEEE Trans. Wireless Commun.*, vol. 20, no. 3, pp. 1950–1962, 2021.
- [30] K.-K. Wong and K.-F. Tong, "Fluid antenna multiple access," *IEEE Trans. Wireless Commun.*, vol. 21, no. 7, pp. 4801–4815, 2022.
- [31] Y. Zeng, B. Duan, and S. Lou, "A fast compensation method for deformed conformal antenna arrays considering mutual coupling effect," *IEEE Trans. Antennas Propag.*, vol. 71, no. 12, pp. 9581–9592, 2023.
- [32] B. C. Ng and C. M. S. See, "Sensor-array calibration using a maximum-likelihood approach," *IEEE Trans. Antennas Propag.*, vol. 44, no. 6, pp. 827–835, 1996.
- [33] B. P. Ng, J. P. Lie, M. H. Er, and A. Feng, "A practical simple geometry and gain/phase calibration technique for antenna Array processing," *IEEE Trans. Antennas Propag.*, vol. 57, no. 7, pp. 1963–1972, 2009.
- [34] D. Fuhrmann, "Estimation of sensor gain and phase," *IEEE Trans. Signal Process.*, vol. 42, no. 1, pp. 77–87, 1994.
- [35] Y. Pan, N. Tai, S. Cheng, and N. Yuan, "Joint estimation of DOA and mutual coupling via block sparse Bayesian learning," in *Proc. IEEE Int. Conf. Signal Process., Commun. Comput. (ICSPCC)*, 2015, pp. 1–6.
- [36] B. Friedlander and A. Weiss, "Direction finding in the presence of mutual coupling," *IEEE Trans. Antennas Propag.*, vol. 39, no. 3, pp. 273–284, 1991.
- [37] J. Dai, X. Bao, N. Hu, C. Chang, and W. Xu, "A recursive RARE algorithm for DOA estimation with unknown mutual coupling," *IEEE Antennas Wireless Propag. Lett.*, vol. 13, pp. 1593–1596, 2014.
- [38] S. K. Garakoui, E. A. M. Klumperink, B. Nauta, and F. E. van Vliet, "Phased-array antenna beam squinting related to frequency dependency of delay circuits," in *Proc. 41th European Microwave Conf.*, 2011, pp. 1304–1307.
- [39] B. Wang, F. Gao, S. Jin, H. Lin, and G. Y. Li, "Spatial- and frequency-wideband effects in millimeter-wave massive MIMO systems," *IEEE Trans. Signal Process.*, vol. 66, no. 13, pp. 3393–3406, 2018.
- [40] L. Xu, L. Cheng, N. Wong, Y.-C. Wu, and H. V. Poor, "Overcoming beam squint in mmwave MIMO channel estimation: A Bayesian multi-band sparsity approach," *IEEE Trans. Signal Process.*, vol. 72, pp. 1219–1234, 2024.
- [41] M. Wang, F. Gao, N. Shlezinger, M. F. Flanagan, and Y. C. Eldar, "A block sparsity based estimator for mmwave massive MIMO channels with beam squint," *IEEE Trans. Signal Process.*, vol. 68, pp. 49–64, 2020.
- [42] A. Garg, S. Srivastava, N. Yadav, A. K. Jagannatham, and L. Hanzo, "Angularly sparse channel estimation in dual- wideband tera-hertz (THz) hybrid MIMO systems relying on Bayesian learning," *IEEE Trans. Commun.*, vol. 72, no. 7, pp. 4384–4400, 2024.
- [43] S. Boyd and L. Vandenberghe, *Convex optimization*. Cambridge University Press, 2004.
- [44] M. Duarte, S. Sarvotham, D. Baron, M. Wakin, and R. Baraniuk, "Distributed compressed sensing of jointly sparse signals," in *Proc. Asilomar Conf. Signals, Syst., Comput.*, 2005, pp. 1537–1541.
- [45] M. Cui and L. Dai, "Channel estimation for extremely large-scale MIMO: Far-field or near-field?" *IEEE Trans. Commun.*, vol. 70, no. 4, pp. 2663–2677, 2022.
- [46] J. Tropp, A. Gilbert, and M. Strauss, "Simultaneous sparse approximation via greedy pursuit," in *Proc. IEEE Int. Conf. Acoustics, Speech, Signal Processing, (ICASSP)*, vol. 5, 2005, pp. v/721–v/724 Vol. 5.
- [47] N. González-Prelcic, H. Xie, J. Palacios, and T. Shimizu, "Wideband channel tracking and hybrid precoding for mmWave MIMO systems," *IEEE Trans. Wireless Commun.*, vol. 20, no. 4, pp. 2161–2174, 2020.
- [48] C.-L. Liu and P. P. Vaidyanathan, "Super nested arrays: linear sparse arrays with reduced mutual coupling—Part I: Fundamentals," *IEEE Trans. Signal Process.*, vol. 64, no. 15, pp. 3997–4012, 2016.